Supporting Information

Novel valproate half-sandwich rhodium and iridium conjugates to fight against multidrug-resistant Gram-positive bacteria

Alicia Marco, ‡[a] Gloria Vigueras, ‡[a] Natalia Busto,*[b,c] Natalia Cutillas,[a] Delia Bautista,[d] and José Ruiz.*[a]

[a.] Departamento de Química Inorgánica, Universidad de Murcia, and Biomedical Research Institute of Murcia (IMIB-Arrixaca), E-30071 Murcia, Spain, Email: jruiz@um.es
[b.] Departamento de Química, Facultad de Ciencias, Universidad de Burgos, Plaza Misael Bañuelos s/n, E-09001, Burgos, Spain, E-mail: nbusto@ubu.es
[c.] Departamento de Ciencias de la Salud. Facultad de Ciencias de la Salud. Universidad de Burgos, Hospital Militar, Paseo de los Comendadores, s/n, 09001 Burgos, Spain.
[d.] SUIC-ACTI, Universidad de Murcia, E-30100 Murcia, Spain.

Table of Contents

1. General Materials and Methods

Materials. $[Rh(\eta^5\text{-}C_5Me_5)Cl_2]_2$ and $IrCl_3$ were used as received (Johnson Matthey). Deuterated solvents were purchased from Euriso-top. Other reagents were commercially available and were used as received.

Physical Measurements. ^1H and $^{13}C\{^1H\}$ NMR spectra were recorded on a Bruker AC 300E, Bruker AV 400, or Bruker AV 600 NMR spectrometer and chemical shifts are reported in ppm and cited relative to $SiMe_4$ and using the residual proton impurities in the solvents for ^1H and $^{13}C\{^1H\}$ NMR spectroscopy. Peak multiplicities are abbreviated as: s = singlet, m = multiplet, d = doublet, t = triplet, dd = doublet of doublet.

The C, H, and N analyses were performed with a Carlo Erba model EA 1108 microanalyzer, with an EAGER 200 software. The combustion of the samples was carried out in the presence of V_2O_5 and MgO as additives. The duration of the analysis was 15 minutes.

The UV/Vis spectra were registered in a Perkin-Elmer Lambda 750 S spectrometer.

ESI mass (positive mode) analyses were carried out in a RP-HPLC/MS TOF 6220 equipped with a double binary pump (model G1312A), degasser, autosampler (model G1329A), diode array detector (model G1315D), and mass detector in series (Agilent Technologies 1200). Chromatographic analyses were performed with a Brisa C18 column (150 mm x 4.6 mm, 5 μm particle size); Teknokroma, Macclesfield, UK. The mobile phase was a mixture of (A) H_2O/HCOOH 0.1% and (B) acetonitrile/HCOOH 0.1%. The flow rate was 06 mL/min in a linear gradient. Chromatograms were recorded at λ=280 nm. The HPLC system was controlled by a ChemStation software (MASS HUNTER). The mass detector was an ion-trap spectrometer equipped with a dual-source electrospray APCI. Mass spectrometry data were acquired in the positive ionization mode. The ionization conditions were adjusted at 3508ºC and 3 kV for capillary temperature and voltage, respectively.

Table S1. HPLC method

Time (min)	0.1 % formic acid in dH_2O	0.1 % formic acid in CH_3CN
0-14	90	10
14-19.5	10	90
19.6-24	90	10

2. Synthesis Procedures

Synthesis of HC^N ligands

Ligand HL1. The synthesis of **HL1** was carried out after slights modifications of bibliography. The diamine (**c**, methyl 3-amino-4-(butylamino)benzoate) was synthetized as previously reported by our group.[1] The condensation of the aldehyde and the diamine (Scheme S1) was carried out following the procedure described in the literature.[2] Briefly, after the solution of $NaHSO_3$ (24.2 mmol, 2.5 g) in 4 mL of water, 4-hiroxybenzaldehyde (2.42 mmol, 295 mg) was added and stirred 30 min at 100 ºC. Then, the diamine **c** (2.42 mmol, 540 mg) was solved in 4 mL of ethanol and added to the reaction mixture that was stirred for 18 h at 80 ºC. The precipitate was filtered and washed with water and hexane. A white solid of **HL1** was obtained (628 mg, yield: 80%).

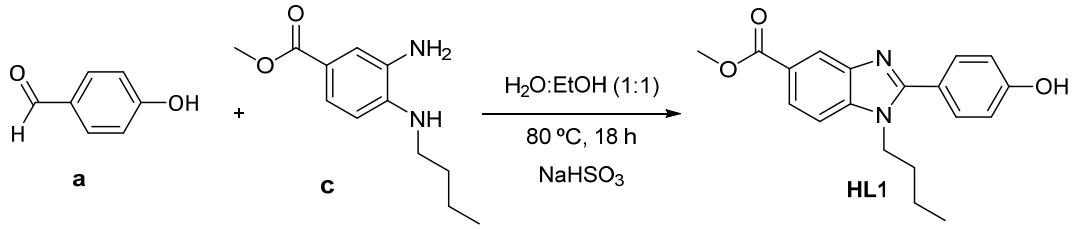

Scheme S1. Synthesis of HC^N ligand **HL1**.

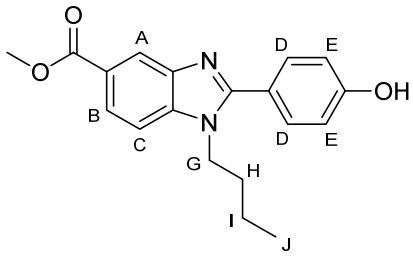

HL1: 80%. 80%. ^{1}H NMR (400 MHz, $CDCl_3$) δ_H /ppm = 11.55 (s, 1H, Ar-OH), 8.54 (d, ^4J = 1.6 Hz, 1H, H_A), 8.06 (dd, ^{34}J = 8.6, 1.6 Hz, 1H, H_B), 7.45 (d, ^3J = 8.6 Hz, 1H, H_C), 7.42 (d, ^3J = 8.7 Hz, 2H, H_D), 6.85 (d, ^3J = 8.7 Hz, 2H, H_E), 4.25 (t, ^3J = 7.7 Hz, 2H, H_G), 3.95 (s, 3H, OCH_3), 1.88 – 1.73 (m, 2H, H_H), 1.36 – 1.22 (m, 2H, H_I), 0.89 (t, ^3J = 7.3 Hz, 3H, H_J). $^{13}C\{^1H\}$ NMR (101 MHz, $CDCl_3$) δ_C /ppm = 167.5, 160.6, 156.1, 140.5, 138.1, 130.8 (C_D), 125.3, 124.8 (C_B), 120.9 (C_A), 118.4, 116.6 (C_E), 110.2 (C_C), 52.3 (OCH_3), 45.1 (C_G), 31.8 (C_H), 20.1 (C_I), 13.7 (C_J). HR-ESMS: *m/z* calc. for $[M+H]^+$ at 325.1547, found at 325.1550. Anal. Calc. for $C_{19}H_{20}N_2O_3$: %C, 70.35; %H, 6.21; %N, 8.64. Found: %C, 70.42; %H, 6.28; %N, 8.56.

Ligand HL2. The synthesis of **HL2** was carried out in different steps (see Scheme S2).[3] In the first step, a solution of valproic acid (13.9 mmol, 1 g) in 6 mL of $SOCl_2$ was stirred at room temperature for 4 h under N_2 atmosphere. The mixture was evaporated and 2 mL of DMF were added. In the second step, 4-hidroxybenzaldehyde (12 mmol, 1.47 g) and triethylamine (72 mmol, 10 mL) were solved in 3 mL of dry DMF. Finally, the solution containing the chloride of valproate was added drop by drop into the solution containing

the aldehyde and stirred overnight at room temperature under inert atmosphere. After the reaction time, 50 mL of DCM were added and the mixture was extracted with 5x100 mL of water. The resulting solid was purified by silica gel column chromatography using DCM:MeOH (95:5) as eluent. A yellow oil of intermediated **b** was obtained (1.46 g, yield: 49%).

The last step consists on the condensation of the aldehyde and the diamine and was carried out following the procedure described in the literature.[2] After the solution of $NaHSO_3$ (24.2 mmol, 2.5 g) in 4 mL of water, intermediated **b** (2.42 mmol, 600 mg) was added and stirred 30 min at 100 ºC. Then, the diamine **c** (2.42 mmol, 540 mg) was solved in 4 mL of ethanol and added to the reaction mixture that was stirred for 18 h at 80 ºC. The mixture was evaporated, solved in 50 mL of DCM and extracted with 50 mL of water. The oil obtained was purified by silica gel column chromatography with EtOAc:Hex (1:3) as eluent and a yellow oil of **HL2** was obtained (818 mg, yield: 75%).

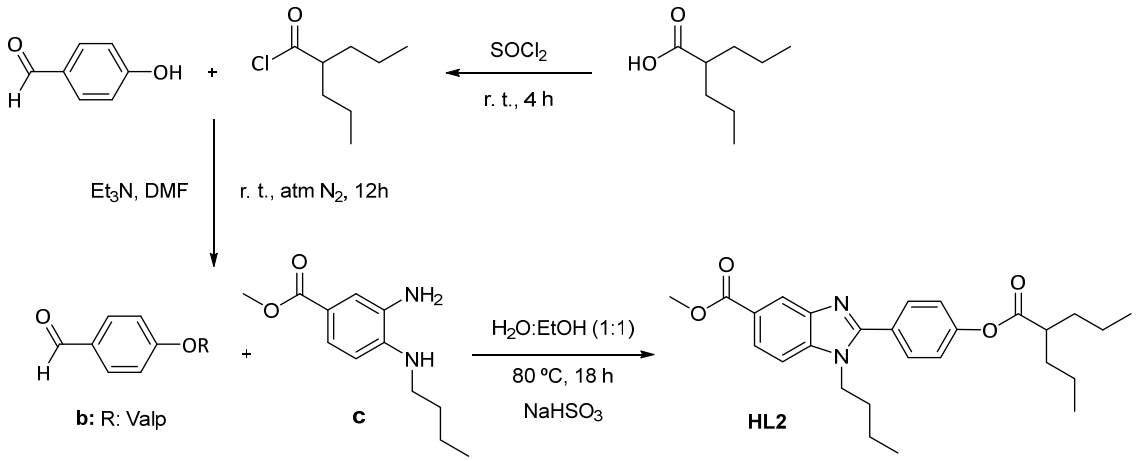

Scheme S2. Synthesis of HC^N ligand **HL2**.

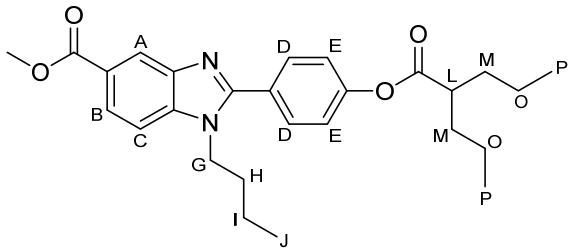

HL2: 75%. ^{1}H NMR (300 MHz, $CDCl_3$) δ_H /ppm = 8.55 (d, ^4J = 1.5 Hz, 1H, H_A), 8.06 (dd, ^{34}J = 8.5, 1.5 Hz, 1H, H_B), 7.77 (d, ^3J = 8.6 Hz, 2H, H_D), 7.45 (d, ^3J = 8.5 Hz, 1H, H_C), 7.28 (d, ^3J = 8.6 Hz, 2H, H_E), 4.27 (t, ^3J = 7.3 Hz, 2H, H_G), 3.96 (s, 3H, OCH_3), 2.72 – 2.59 (m, 1H, H_L), 1.89 – 1.69 (m, 4H, $H_{H+M/N}$), 1.66 – 1.53 (m, 2H, $H_{M/N}$), 1.52 – 1.38 (m, 4H, H_O), 1.37 – 1.22 (m, 2H, H_I), 0.98 (t, ^3J = 7.2 Hz, 6H, H_P), 0.89 (t, ^3J = 7.2 Hz, 3H, H_J). $^{13}C\{^1H\}$ NMR (75 MHz, $CDCl_3$) δ_C /ppm = 174.8, 167.5, 154.4, 152.7, 138.6, 130.8 (C_D), 126.8, 125.3, 124.9 (C_B), 122.5 (C_E), 122.1 (C_A), 110.1 (C_C), 52.3 (OCH_3),

45.6 (C_L), 45.1 (C_G), 34.8 (C_{M+N}), 32.0 (C_H), 20.9 (C_O), 20.1 (C_I), 14.2 (C_P), 13.7 (C_J). HR-ESMS: *m/z* calc. for $[M+H]^+$ at 451.2591, found at 451.2595. Anal. Calc. for $C_{27}H_{34}N_2O_4$: %C, 71.97; %H, 7.61; %N, 6.22. Found: %C, 72.06; %H, 7.53; %N, 6.30.

*Synthesis of [MCp*Cl(C^N)] (M = Ir, Rh) complexes*

All complexes were synthetized under an N_2 atmosphere using standard Schlenk techniques as previously reported (Scheme S3).[4] $[Ir(\eta^5\text{-}C_5Me_5)Cl_2]_2$ was synthetized by reaction of $IrCl_3$ (1 eq.) and pentamethylcyclopentadienyl (1.4 eq.) in methanol for 24 h at room temperature. The orange solid was isolated and dry under vacuum. For the synthesis of the complexes, a solution of the dimer (1 eq.), the corresponding ligand, **HL1** or **HL2** (2 eq.) and sodium acetate (2.5 eq.) in 10 mL of CH_2Cl_2 was stirred for 24 h at room temperature. The precipitate was filtered and washed with diethyl ether. A pure yellow/orange solid was obtained for all the complexes.

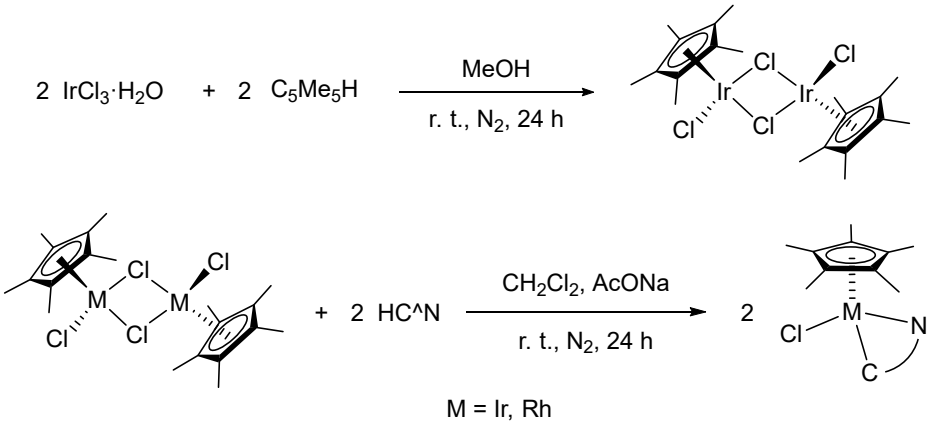

Scheme S3. General procedure for the synthesis of complexes **IrL1-2** and **RhL1-2**.

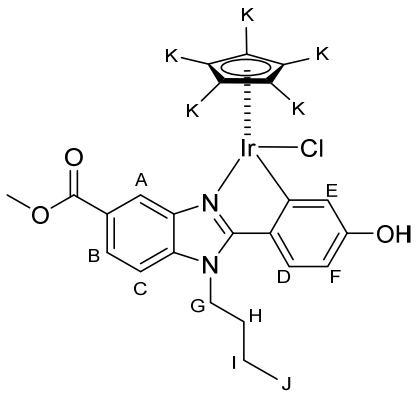

IrL1: 87%. ^{1}H NMR (600 MHz, DMF-d_7) δ_H /ppm = 9.97 (s, 1H, Ar-OH), 8.35 (d, ^4J = 1.8 Hz, 1H, H_A), 7.99 (dd, ^{34}J = 8.6, 1.8 Hz, 1H, H_B), 7.89 (d, ^3J = 8.6 Hz, 1H, H_C), 7.83 (d, ^3J = 8.5 Hz, 1H, H_D), 7.57 (d, ^4J = 2.5 Hz, 1H, H_E), 6.65 (dd, ^{34}J = 8.5, 2.5 Hz, 1H, H_F), 4.75 (t, ^3J = 7.6 Hz, 2H, H_G), 3.99 (s, 3H, OCH_3), 1.95 – 1.88 (m, 2H, H_H), 1.78 (s, 15H, H_K), 1.52 – 1.44 (m, 2H, H_I), 0.94 (t, ^3J = 7.4 Hz, 3H, H_J). $^{13}C\{^1H\}$ NMR (151 MHz, DMF-d_7) δ_C /ppm = 169.2, 167.0, 164.3, 160.2, 139.9, 139.7, 126.5 (C_D), 125.4, 124.6, 123.9 (C_E), 123.6 (C_B), 117.9 (C_A), 111.1 (C_C), 110.16 (C_F), 88.2, 52.1 (OCH_3), 44.6 (C_G), 31.9 (C_H), 19.9 (C_I), 13.6 (C_J), 9.4 (C_K). HR ESI-MS: *m/z* calc. for $[M\text{-}Cl]^+$ at 651.2199, found at 651.2191. Anal. Calc. for $C_{29}H_{34}ClIrN_2O_3$: %C, 50.76; %H, 4.99; %N, 4.08. Found: %C, 50.77; %H, 4.83; %N, 4.01.

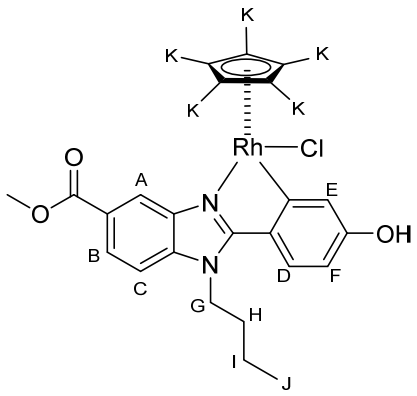

RhL1: 67%. ^{1}H NMR (600 MHz, DMF-d_7) δ_H /ppm = 9.99 (s, 1H, Ar-OH), 8.40 (d, ^{4}J = 1.5 Hz, 1H, H_A), 7.98 (dd, ^{34}J = 8.6, 1.5 Hz, 1H, H_B), 7.90 (d, ^{3}J = 8.6 Hz, 1H, H_C), 7.78 (d, ^{3}J = 8.5 Hz, 1H, H_D), 7.55 (d, ^{4}J = 2.4 Hz, 1H, H_E), 6.66 (dd, ^{34}J = 8.5, 2.4 Hz, 1H, H_F), 4.77 – 4.67 (m, 2H, H_G), 4.00 (s, 3H, OCH_3), 1.94 – 1.86 (m, 2H, H_H), 1.70 (s, 15H, H_K), 1.50 – 1.42 (m, 2H, H_I), 0.94 (t, ^{3}J = 7.4 Hz, 3H, H_J). ^{13}C{^{1}H} NMR (151 MHz, DMF-d_7) δ_C /ppm = 167.1, 160.3, 158.9, 140.2, 140.1, 125.9 (C_D), 125.8, 124.8 (C_E), 124.5, 123.5 (C_B), 118.2 (C_A), 111.1 (C_C), 110.8 (C_F), 95.8, 95.8, 52.1 (OCH_3), 44.7 (C_G), 31.9 (C_H), 19.9 (C_I), 13.6 (C_J), 9.4 (C_K). HR ESI-MS: *m/z* calc. for [M-Cl]$^{+}$ at 561.1625, found at 561.1616. Anal. Calc. for $C_{29}H_{34}ClN_2O_3Rh$: %C, 58.35; %H, 5.74; %N, 4.69. Found: %C, 58.40; %H, 5.57; %N, 4.57.

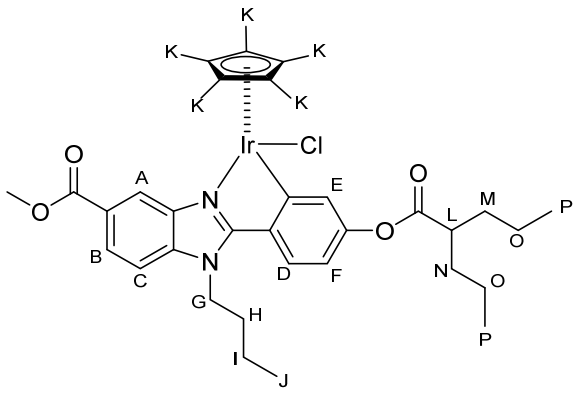

IrL2: 46%. ^{1}H NMR (600 MHz, $CDCl_3$) δ_H /ppm = 8.44 (d, ^{4}J = 1.5 Hz, 1H, H_A), 8.03 (dd, ^{34}J = 8.6, 1.5 Hz, 1H, H_B), 7.70 (dd, ^{34}J = 8.4, 2.2 Hz, 2H, $H_{D,E}$), 7.39 (d, ^{3}J = 8.6 Hz, 1H, H_C), 6.82 (dd, ^{34}J = 8.4, 2.2 Hz, 1H, H_F), 4.58 – 4.41 (m, 2H, H_G), 3.98 (s, 3H, OCH_3), 2.70 – 2.64 (m, 1H, H_L), 2.03 – 1.95 (m, 2H, H_H), 1.85 – 1.80 (m, 2H, $H_{M/N}$), 1.78 (s, 15H, H_K), 1.64 – 1.56 (m, 2H, $H_{M/N}$), 1.55 – 1.44 (m, 6H, H_{I+O}), 1.04 – 0.97 (m, 9H, H_{J+P}). ^{13}C{^{1}H} NMR (151 MHz, $CDCl_3$) δ_C /ppm = 175.5, 167.9, 167.2, 163.1, 152.3, 139.4, 139.3, 131.2, 130.1 ($C_{D/E}$), 125.4, 125.0 ($C_{D/E}$), 124.6 (C_B), 119.1 (C_A), 115.4 (C_F), 109.9 (C_C), 88.6, 52.4 (OCH_3), 45.8 (C_L), 45.1 (C_G), 35.0 ($C_{M/N}$), 34.9 ($C_{M/N}$), 31.9 (C_H), 20.9, 20.9 ($C_{I/O}$), 20.4 ($C_{I/O}$), 14.2 ($C_{J/P}$), 13.9 ($C_{J/P}$), 9.7 (C_K). HR ESI-MS: *m/z* calc. for [M-Cl]$^{+}$ at 777.3243, found at 777.3241. Anal. Calc. for $C_{37}H_{48}ClIrN_2O_4$: %C, 54.70; %H, 5.96; %N, 3.45. Found: %C, 54.68; %H, 5.87; %N, 3.42.

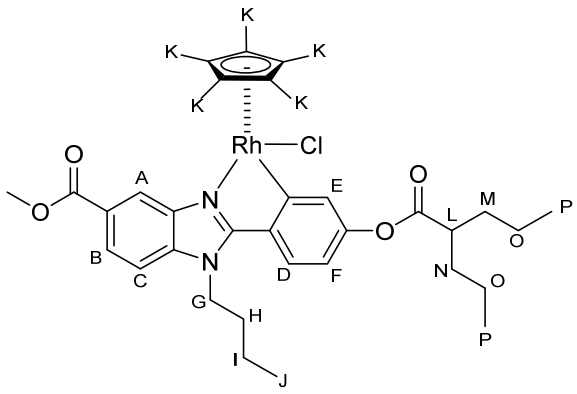

RhL2: 34%. ^{1}H NMR (401 MHz, $CDCl_3$) δ_H /ppm = 8.50 (d, ^{4}J = 1.6 Hz, 1H, H_A), 8.02 (dd, ^{34}J = 8.6, 1.6 Hz, 1H, H_B), 7.71 (d, ^{4}J = 2.3 Hz, 1H, H_E), 7.65 (d, ^{3}J = 8.4 Hz, 1H, H_D), 7.40 (d, ^{3}J = 8.6 Hz, 1H, H_C), 6.84 (dd, ^{43}J = 8.4, 2.3 Hz, 1H, H_F), 4.53 – 4.38 (m, 2H, H_G), 3.98 (s, 3H, OCH_3), 2.72 – 2.63 (m, 1H, H_L), 2.02 – 1.91 (m, 2H, H_H), 1.87 – 1.76 (m, 2H, $H_{M/N}$), 1.70 (s, 15H, H_K), 1.60 – 1.56 (m, 2H, $H_{M/N}$), 1.54 – 1.44 (m, 6H, H_{I+O}), 1.04 – 0.97 (m, 9H, H_{J+P}). $^{13}C\{^{1}H\}$ NMR (101 MHz, $CDCl_3$) δ_C /ppm = 175.5, 167.3, 159.0, 151.2, 139.8, 139.6, 131.7, 131.0 (C_E), 125.2, 124.6 (C_B), 124.5 (C_D), 119.5 (C_A), 116.3 (C_F), 109.9 (C_C), 96.2, 96.2, 52.4 (OCH_3), 45.8 (C_L), 45.2 (C_G), 34.9 ($C_{M/N}$), 34.9 ($C_{M/N}$), 31.9 (C_H), 20.9, 20.9 ($C_{I/O}$), 20.4 ($C_{I/O}$), 14.2 ($C_{J/P}$), 13.9 ($C_{J/P}$), 9.9 (C_K). HR ESI-MS: *m/z* calc. for $[M\text{-}Cl]^+$ at 687.2665, found at 687.2681. Anal. Calc. for $C_{37}H_{48}ClN_2O_4Rh$: %C, 61.45; %H, 6.69; %N, 3.87. Found: %C, 61.41; %H, 6.65; %N, 3.72.

3. NMR spectra of new compounds

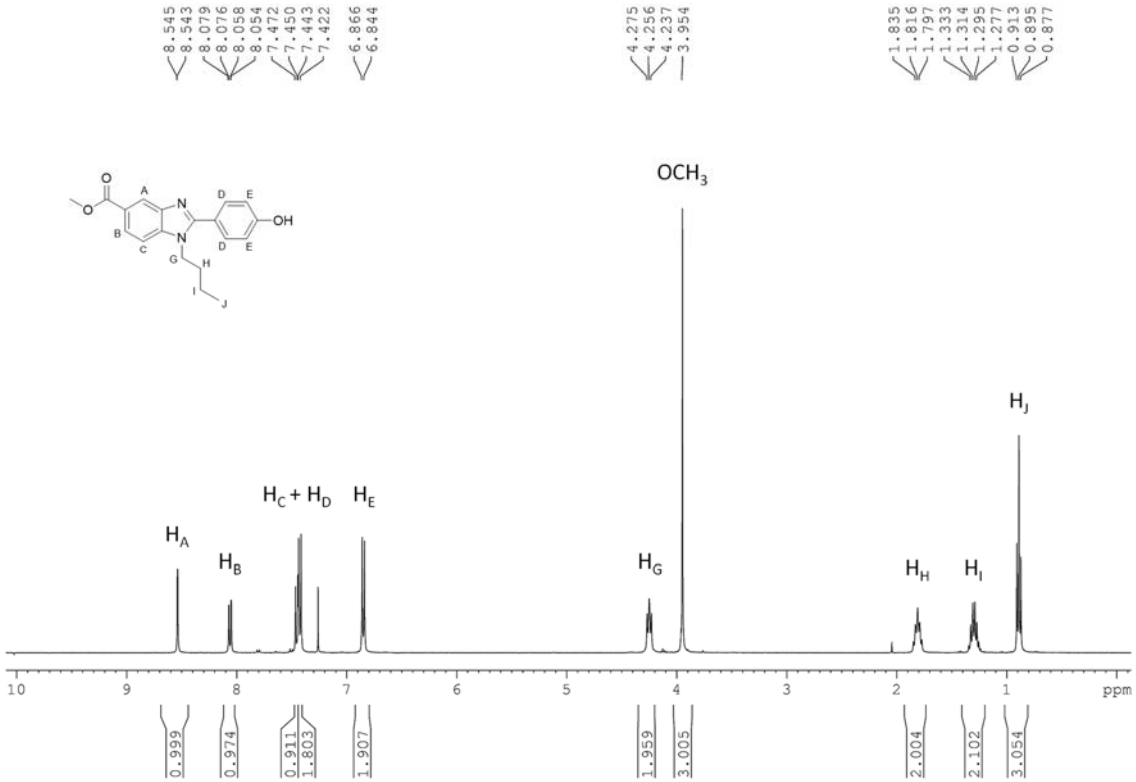

Figure S1. ^{1}H NMR spectrum of **HL1**, 400 MHz, $CDCl_3$.

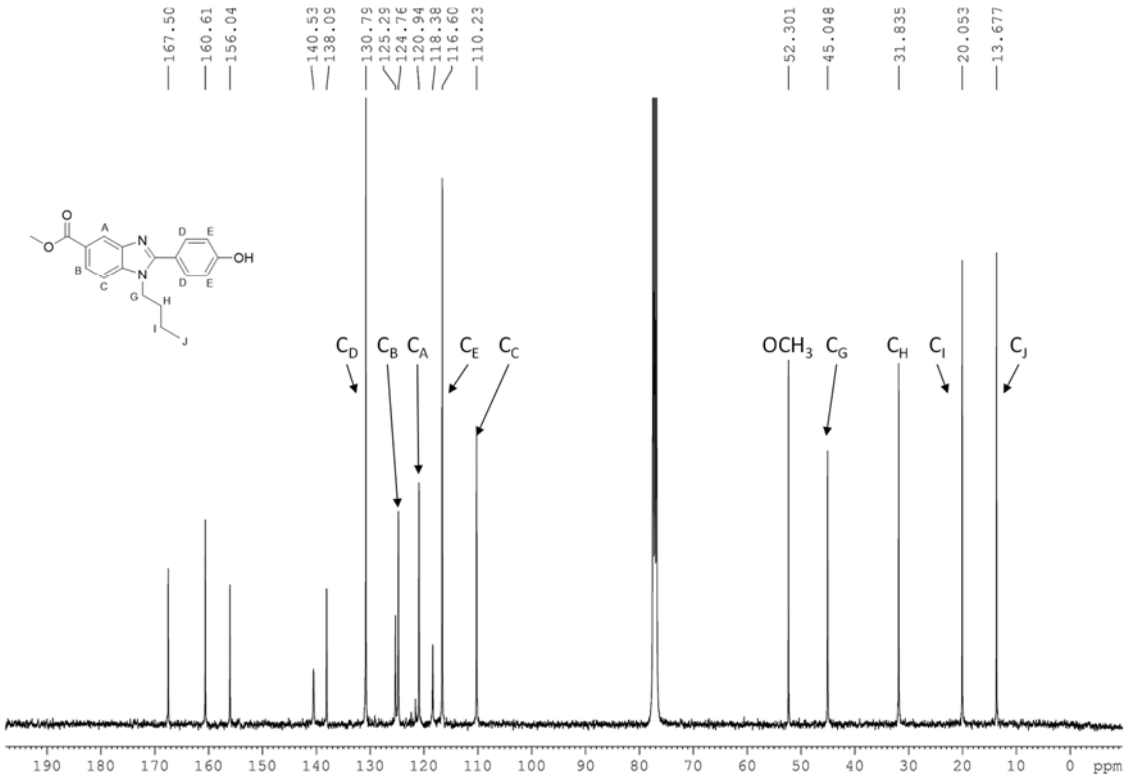

Figure S2. ^{13}C NMR spectrum of **HL1**, 101 MHz, $CDCl_3$.

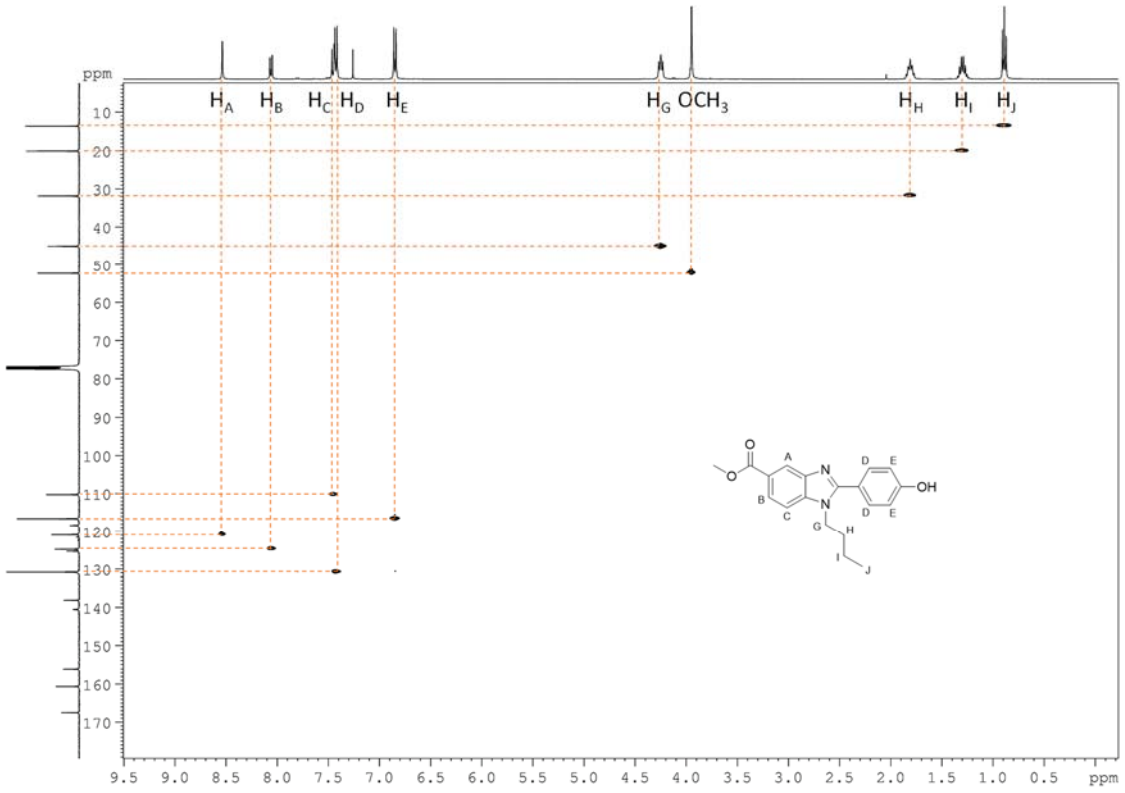

Figure S3. HSQC 2D ^{1}H-^{13}C NMR spectrum of **HL1**, 400 MHz, $CDCl_3$.

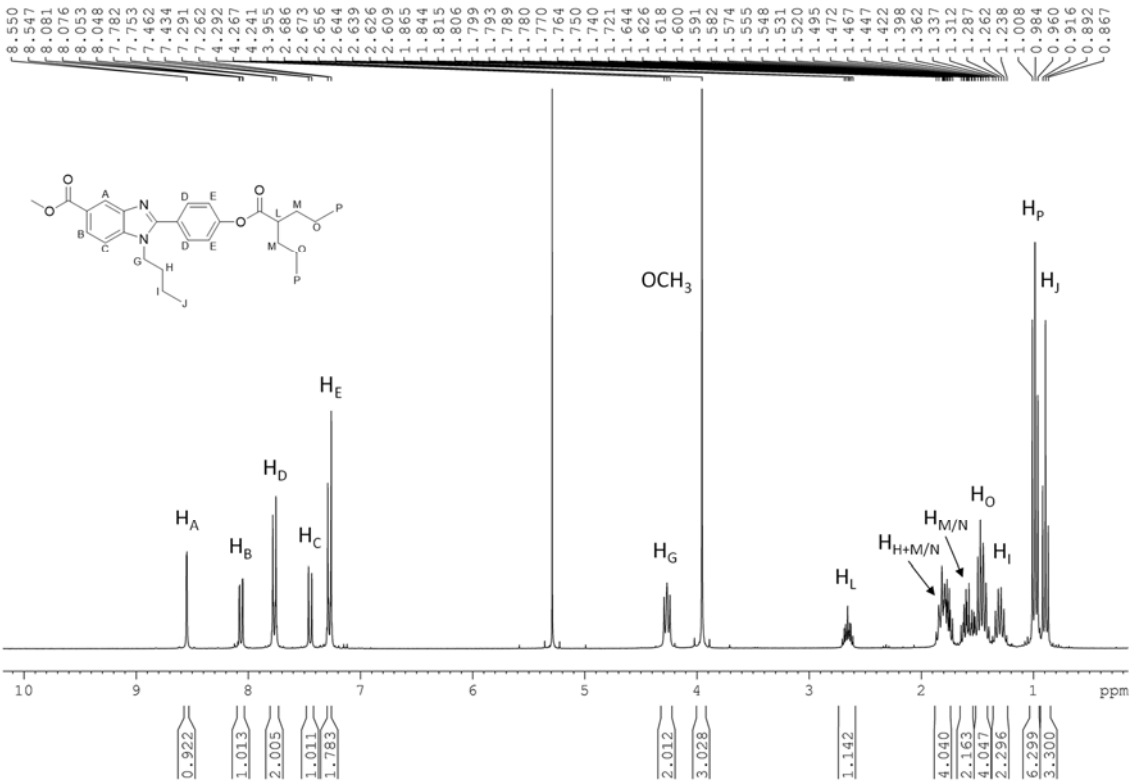

Figure S4. ^{1}H NMR spectrum of **HL2**, 300 MHz, $CDCl_3$.

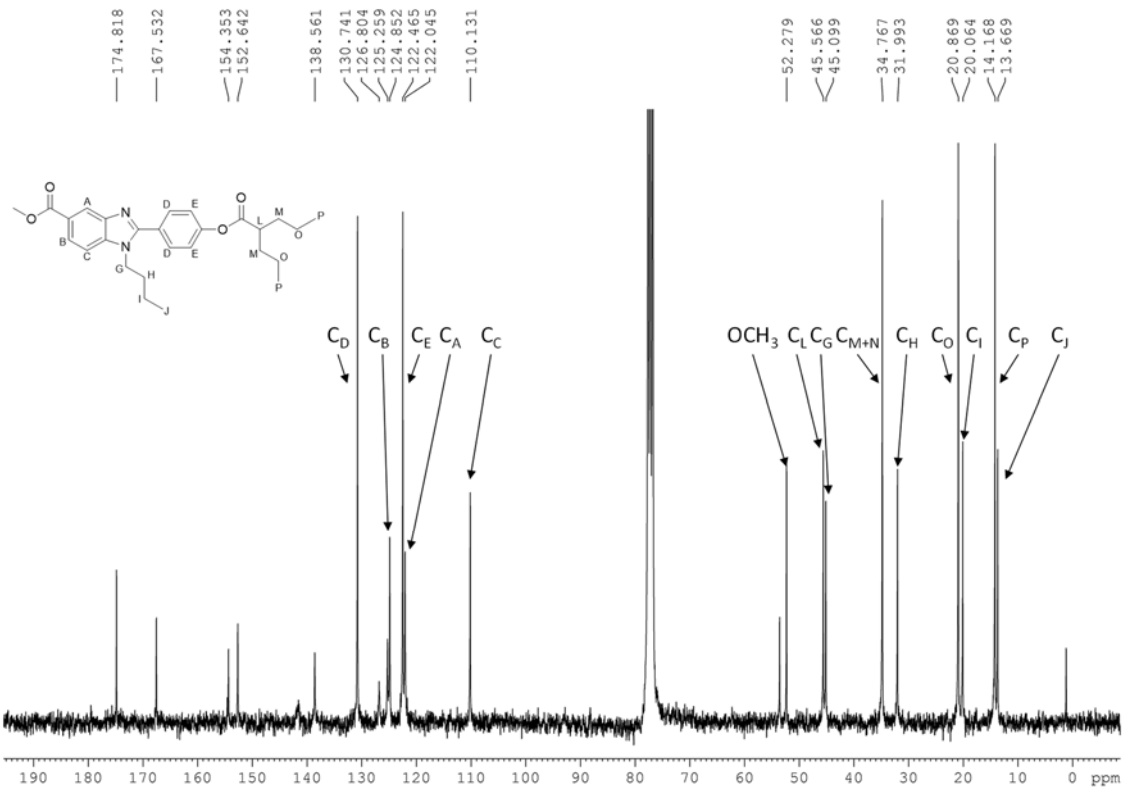

Figure S5. ^{13}C NMR spectrum of **HL2**, 75 MHz, $CDCl_3$.

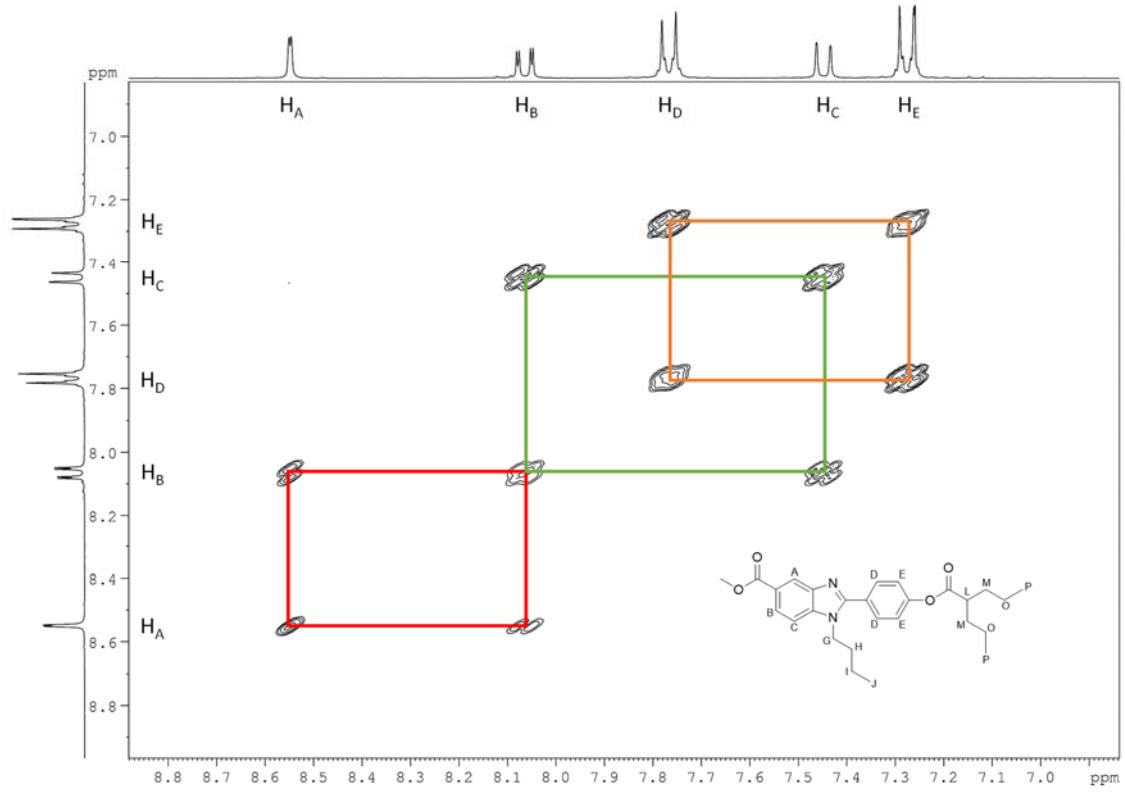

Figure S6. COSY 2D ^{1}H-^{1}H NMR spectrum of **HL2**, 300 MHz, $CDCl_3$.

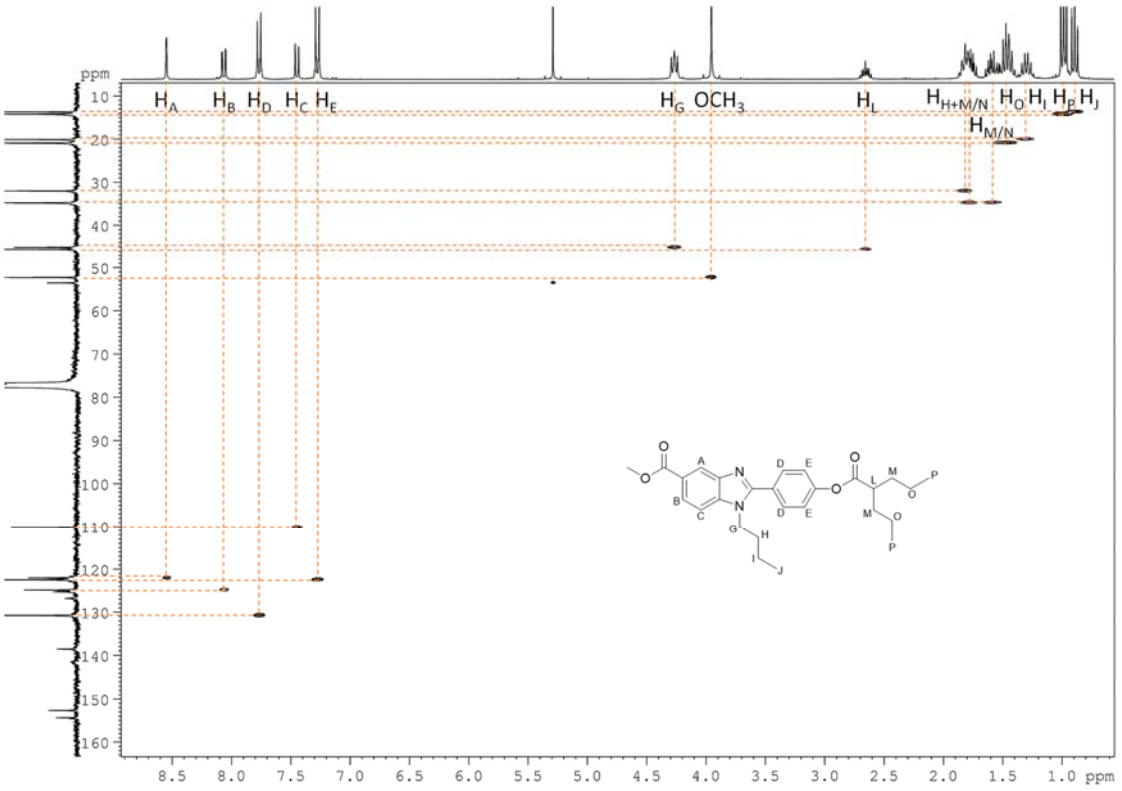

Figure S7. HSQC 2D ^{1}H-^{13}C NMR spectrum of **HL2**, 300 MHz, $CDCl_3$.

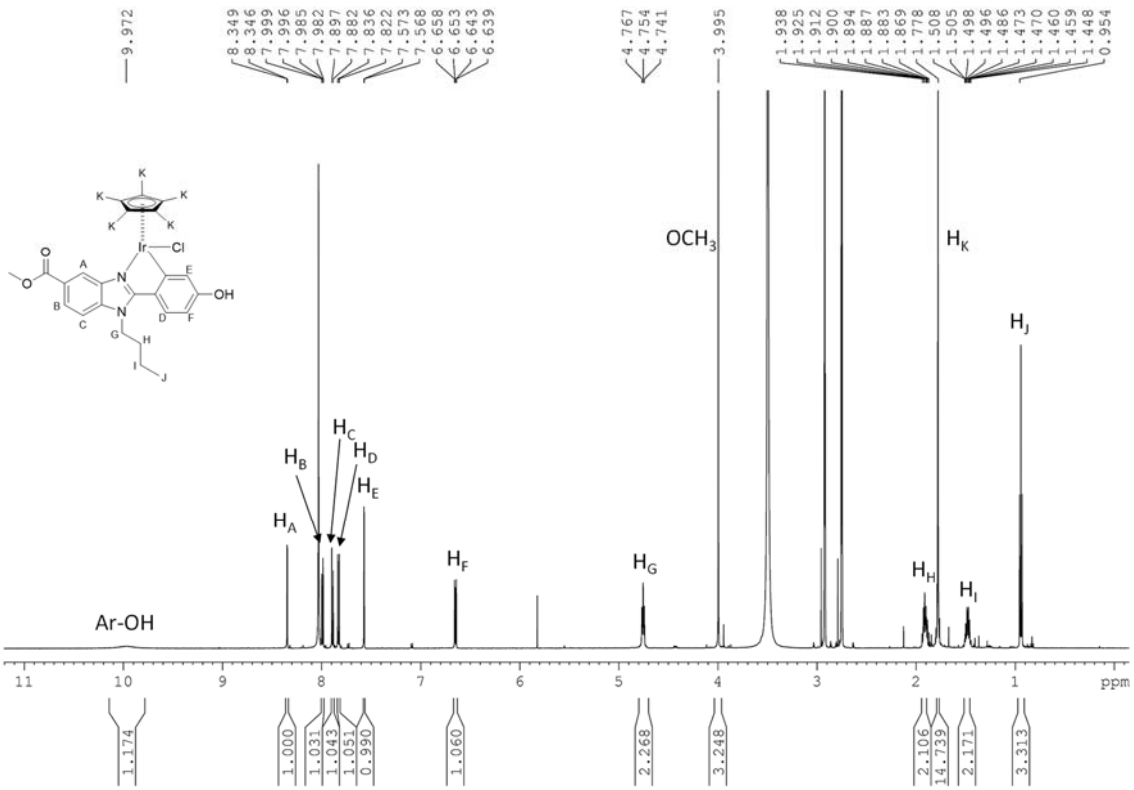

Figure S8. ^{1}H NMR spectrum of **IrL1**, 600 MHz, DMF-d_7.

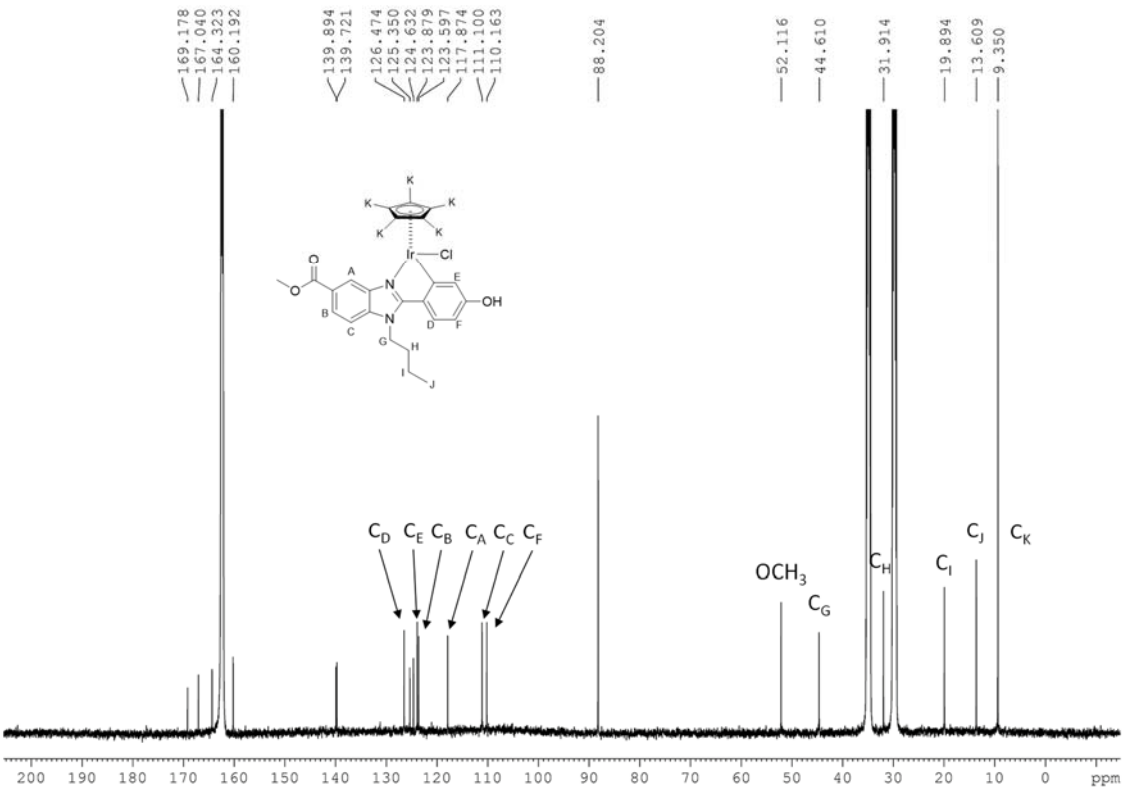

Figure S9. ^{13}C NMR spectrum of **IrL1**, 151 MHz, DMF-d_7.

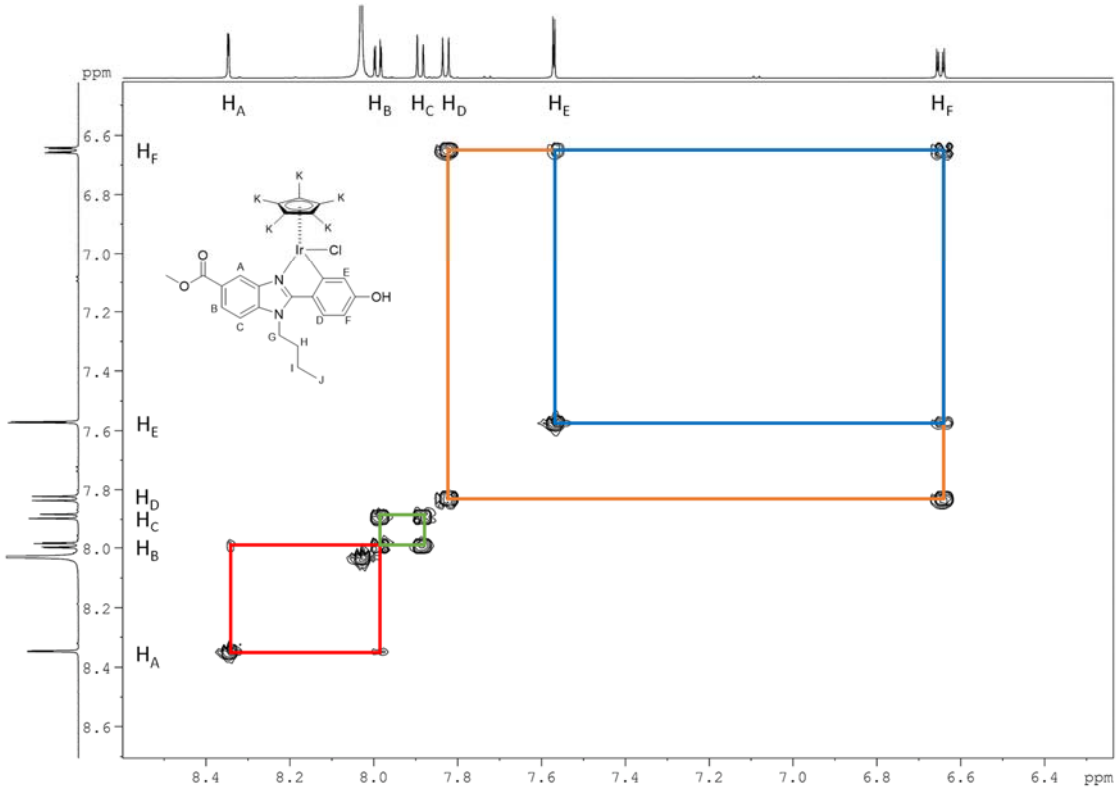

Figure S10. COSY 2D ^{1}H-^{1}H NMR spectrum of **IrL1**, 600 MHz, DMF-d_7.

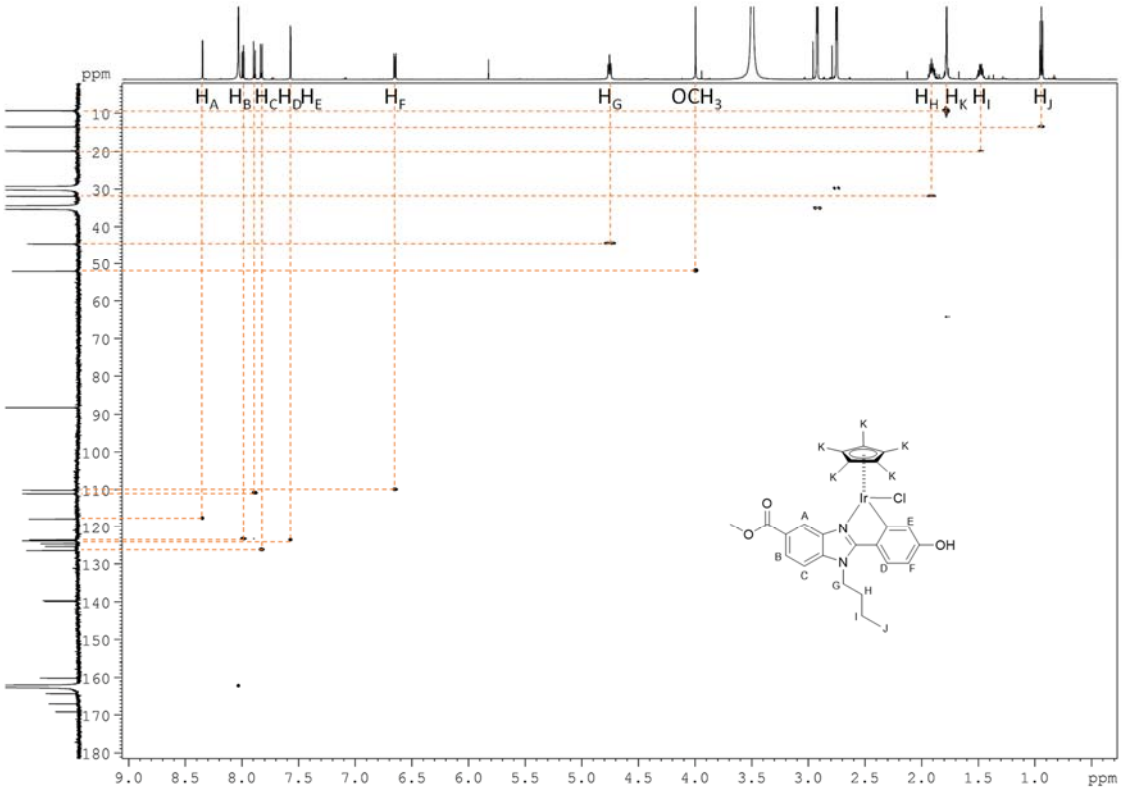

Figure S11. HSQC 2D ^{1}H-^{13}C NMR spectrum of **IrL1**, 600 MHz, DMF-d_7.

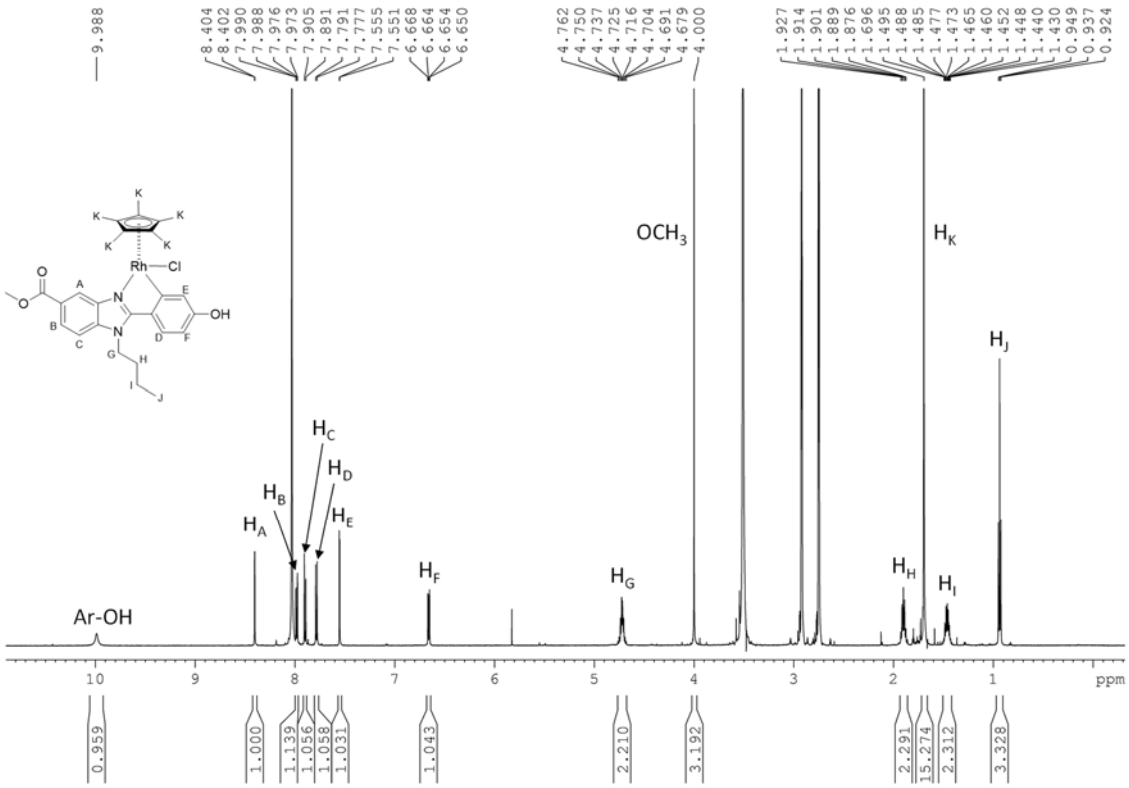

Figure S12. ^{1}H NMR spectrum of **RhL1**, 600 MHz, DMF-d_7.

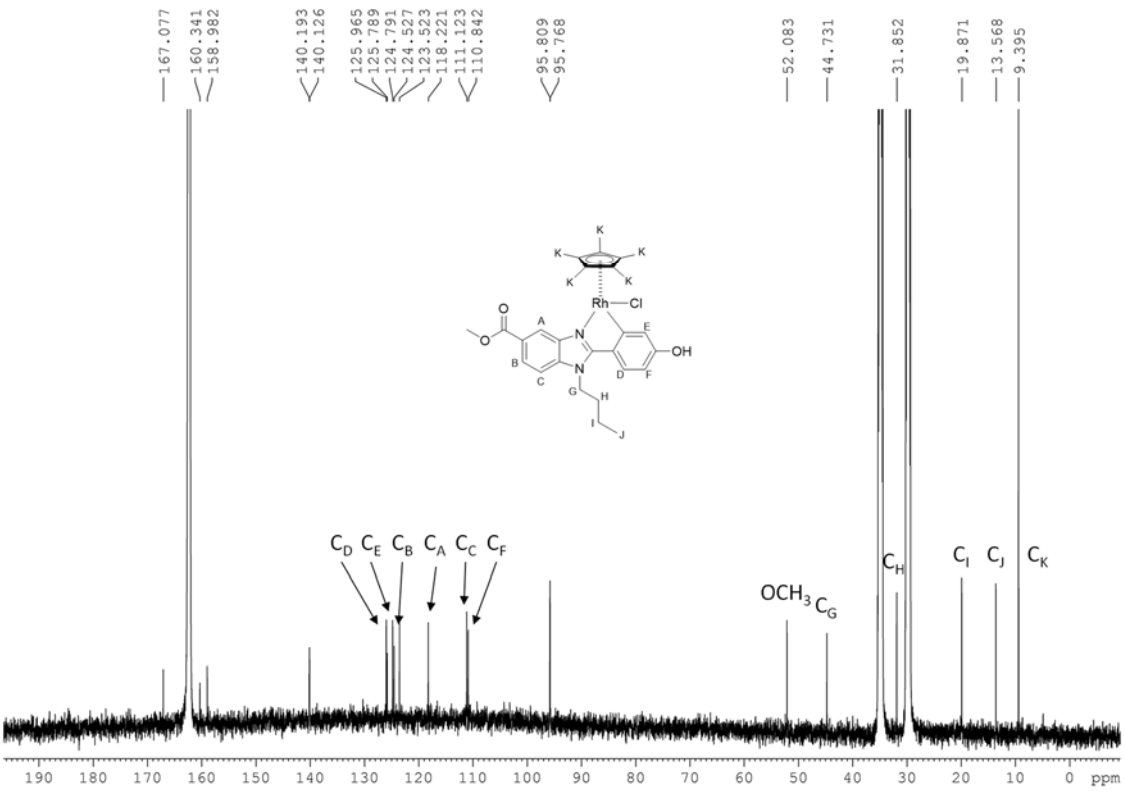

Figure S13. ^{13}C NMR spectrum of **RhL1**, 151 MHz, DMF-d_7.

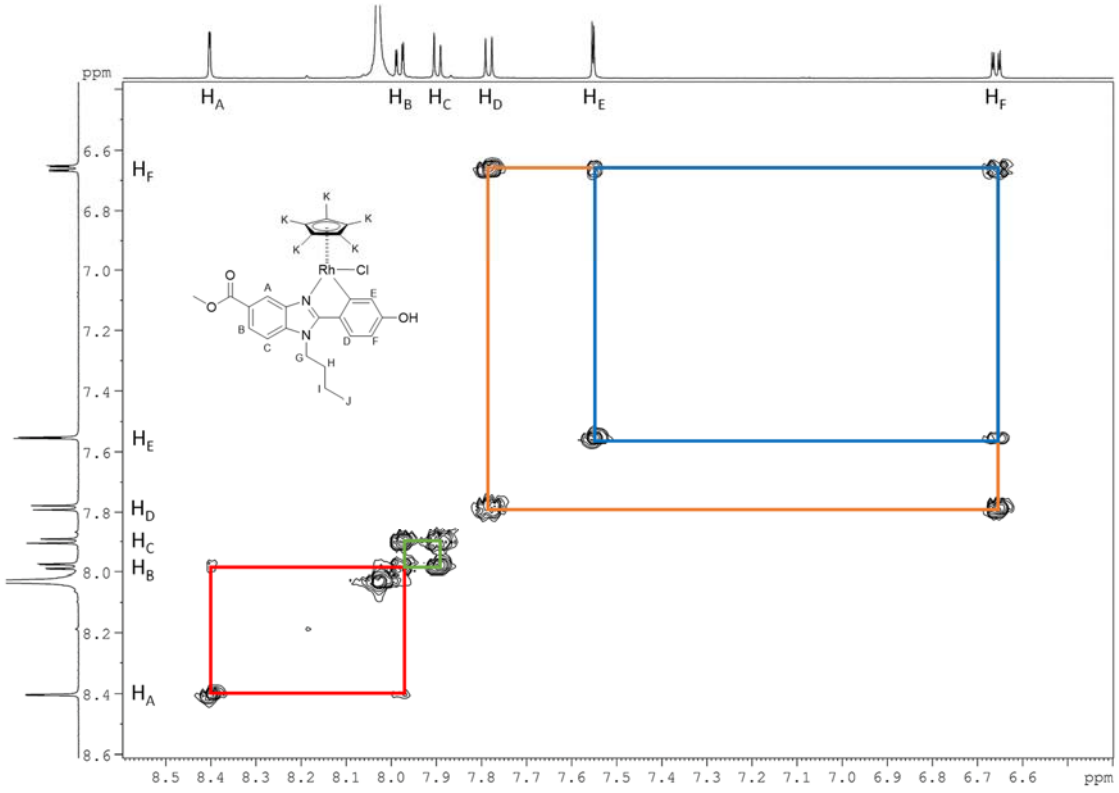

Figure S14. COSY 2D ^{1}H-^{1}H NMR spectrum of **RhL1**, 600 MHz, DMF-d_7.

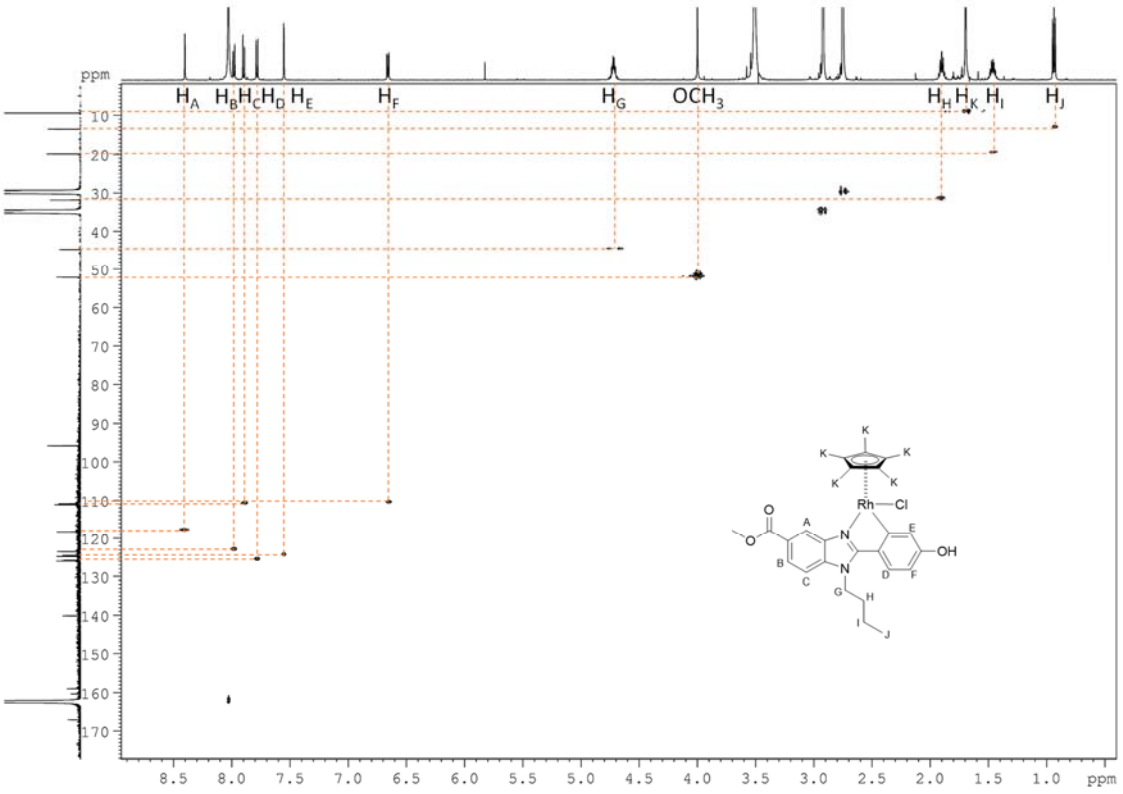

Figure S15. HSQC 2D ^{1}H-^{13}C NMR spectrum of **RhL1**, 600 MHz, DMF-d_7.

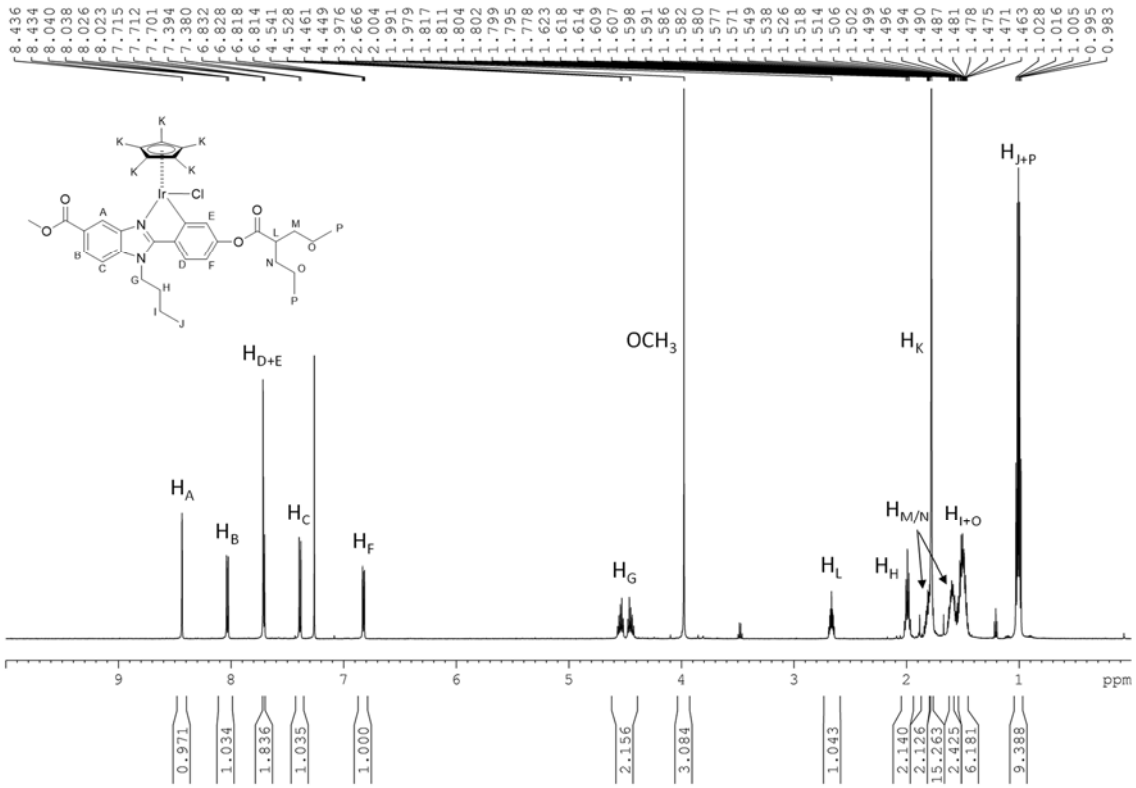

Figure S16. ^{1}H NMR spectrum of **IrL2**, 600 MHz, $CDCl_3$.

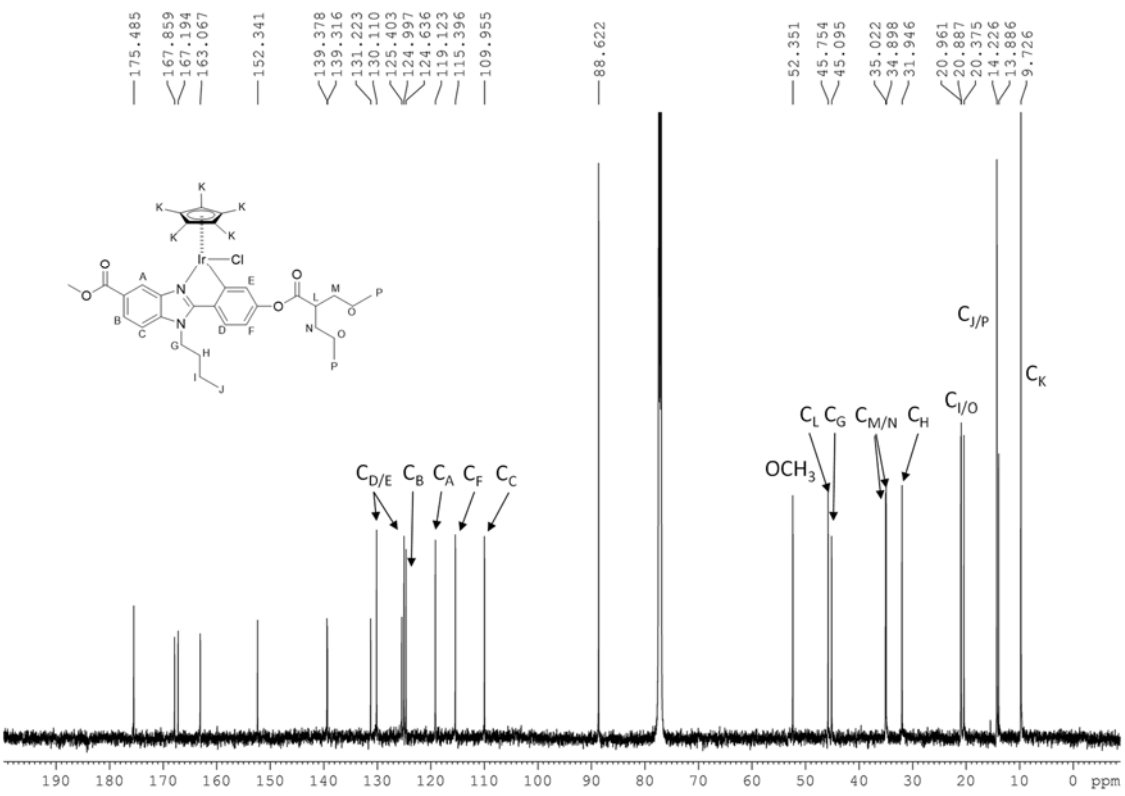

Figure S17. ^{13}C NMR spectrum of **IrL2**, 151 MHz, $CDCl_3$.

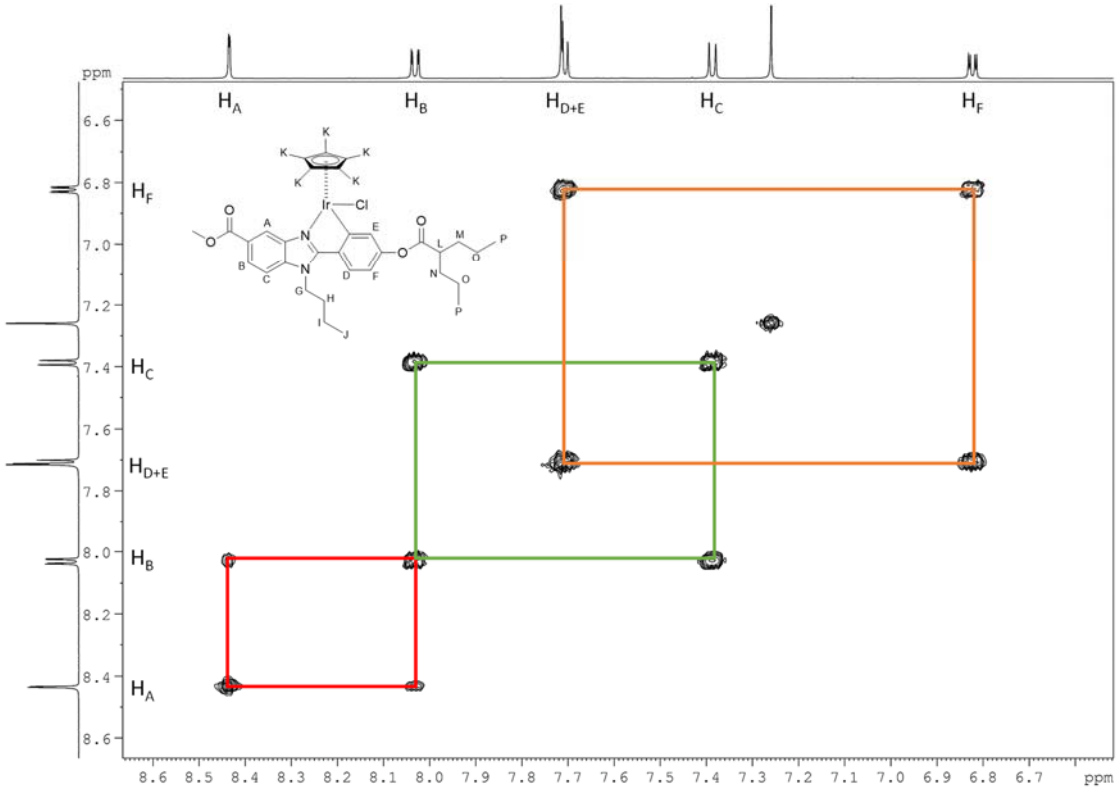

Figure S18. COSY 2D ^{1}H-^{1}H NMR spectrum of **IrL2**, 600 MHz, $CDCl_3$.

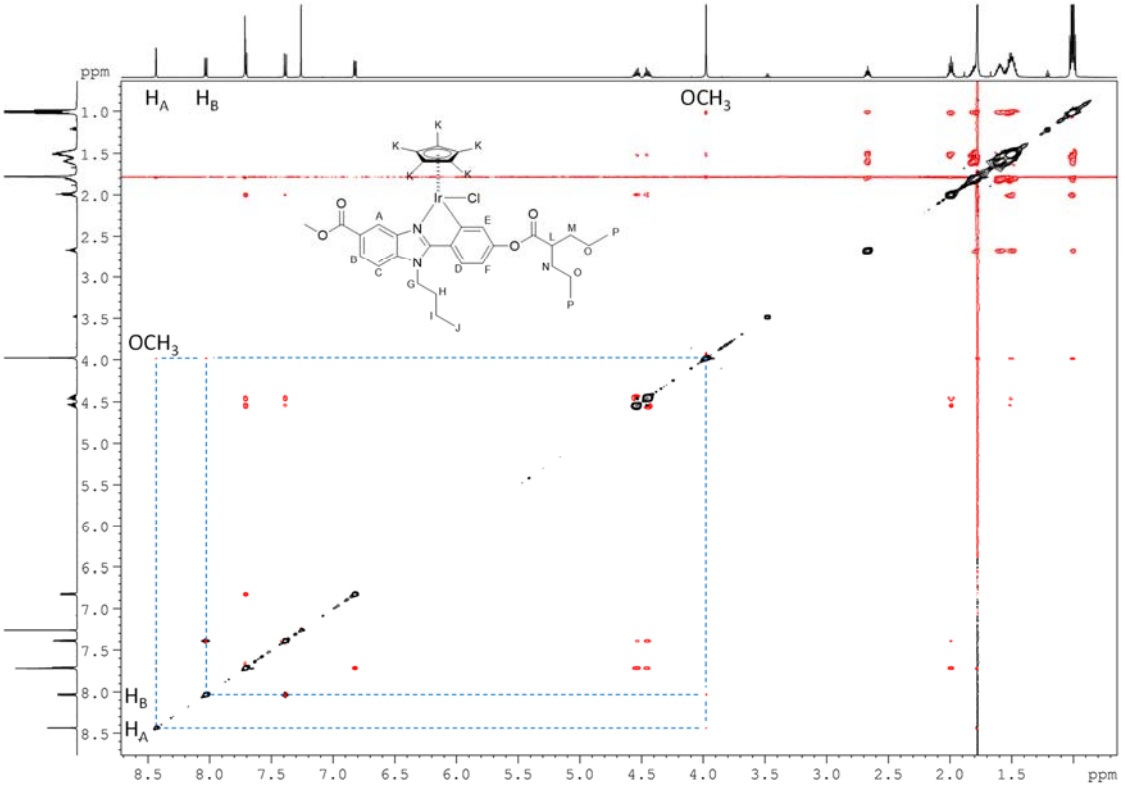

Figure S19. NOESY 2D ^{1}H-^{1}H NMR spectrum of **IrL2**, 600 MHz, $CDCl_3$.

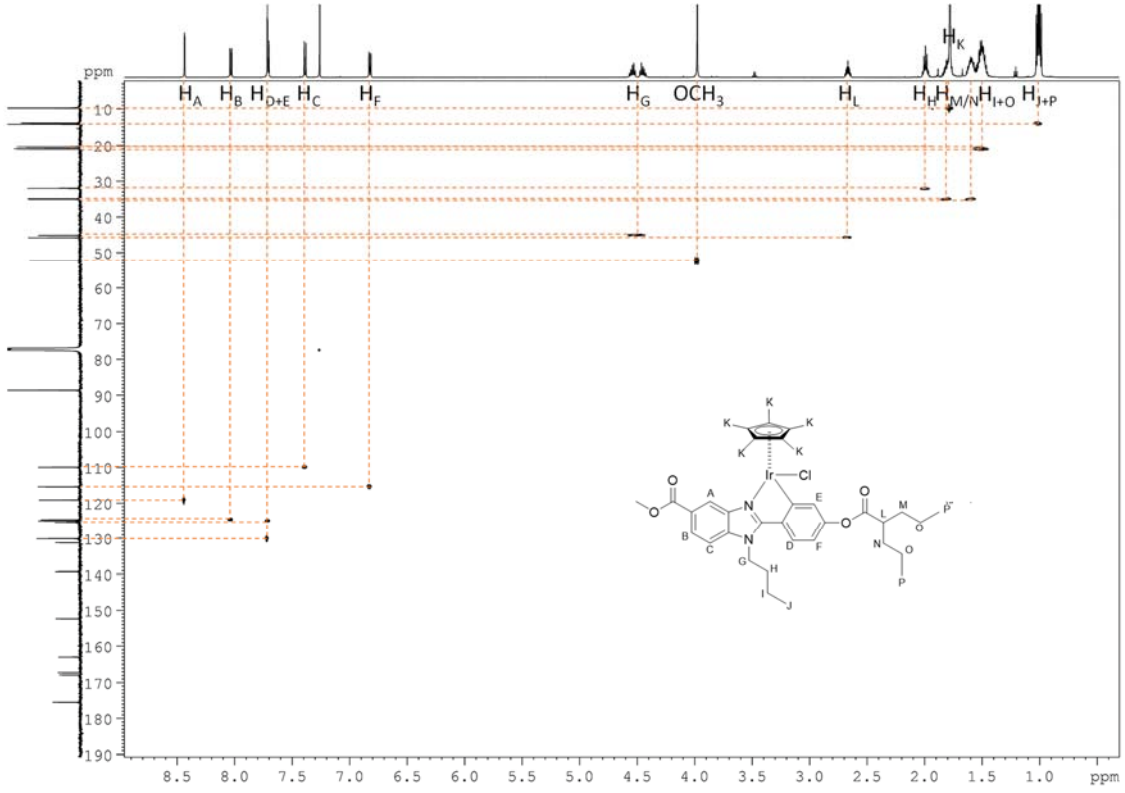

Figure S20. HSQC 2D ^{1}H-^{13}C NMR spectrum of **IrL2**, 600 MHz, $CDCl_3$.

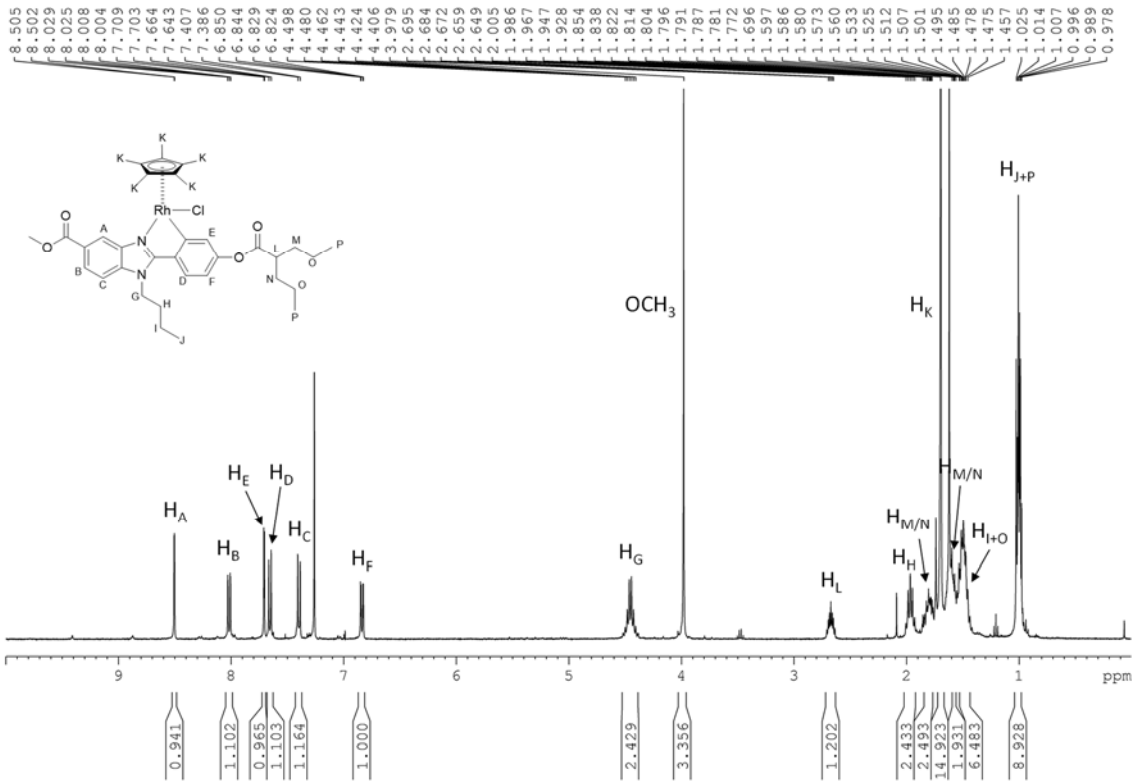

Figure S21. ^{1}H NMR spectrum of **RhL2**, 400 MHz, $CDCl_3$.

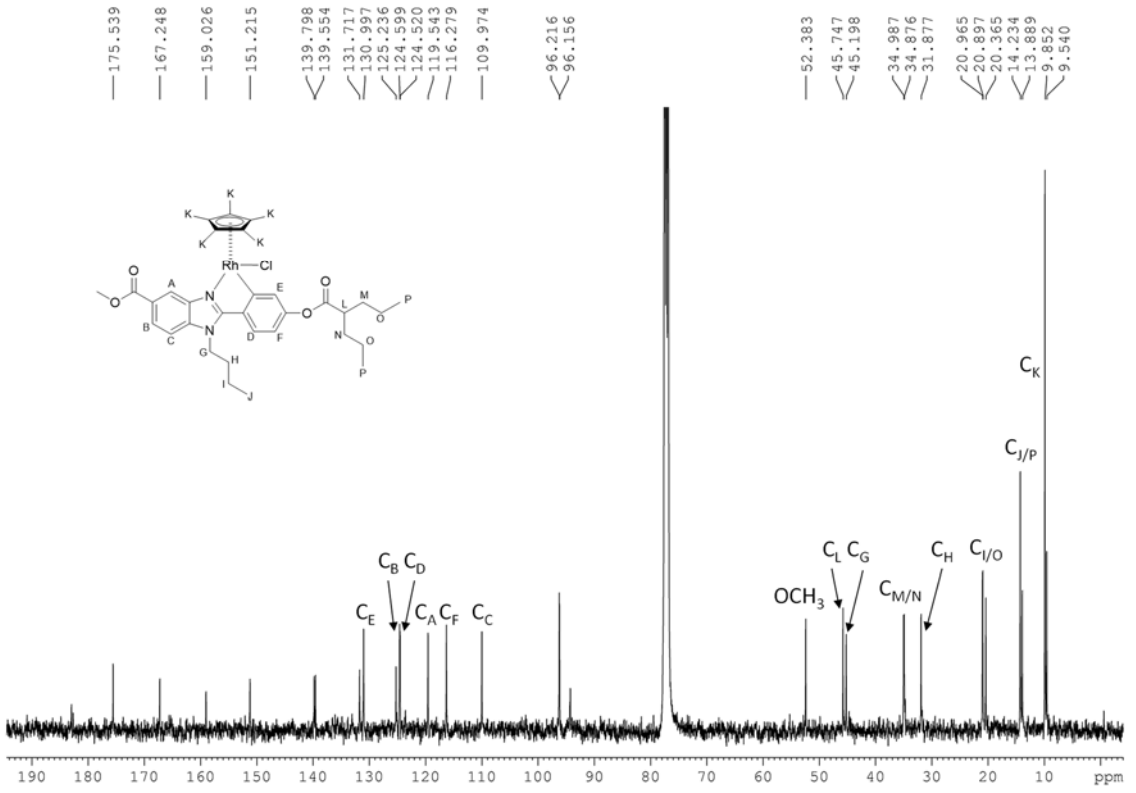

Figure S22. ^{13}C NMR spectrum of **RhL2**, 101 MHz, $CDCl_3$.

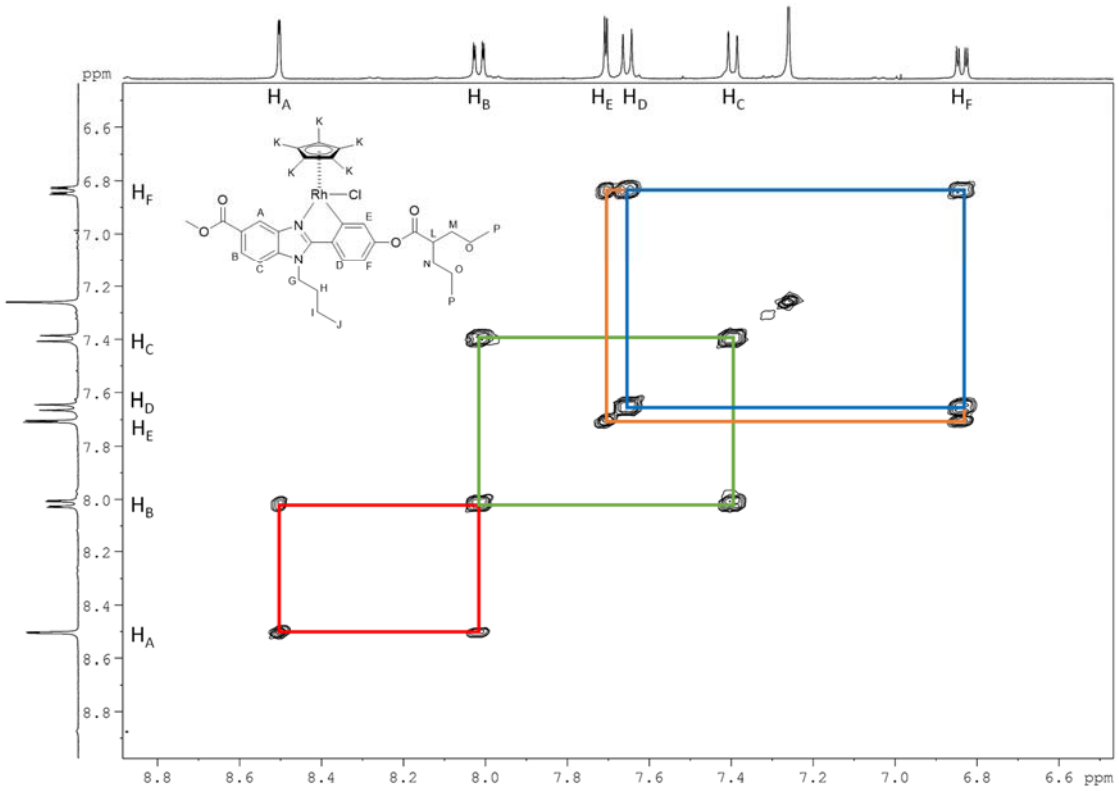

Figure S23. COSY 2D ^{1}H-^{1}H NMR spectrum of **RhL2**, 400 MHz, $CDCl_3$.

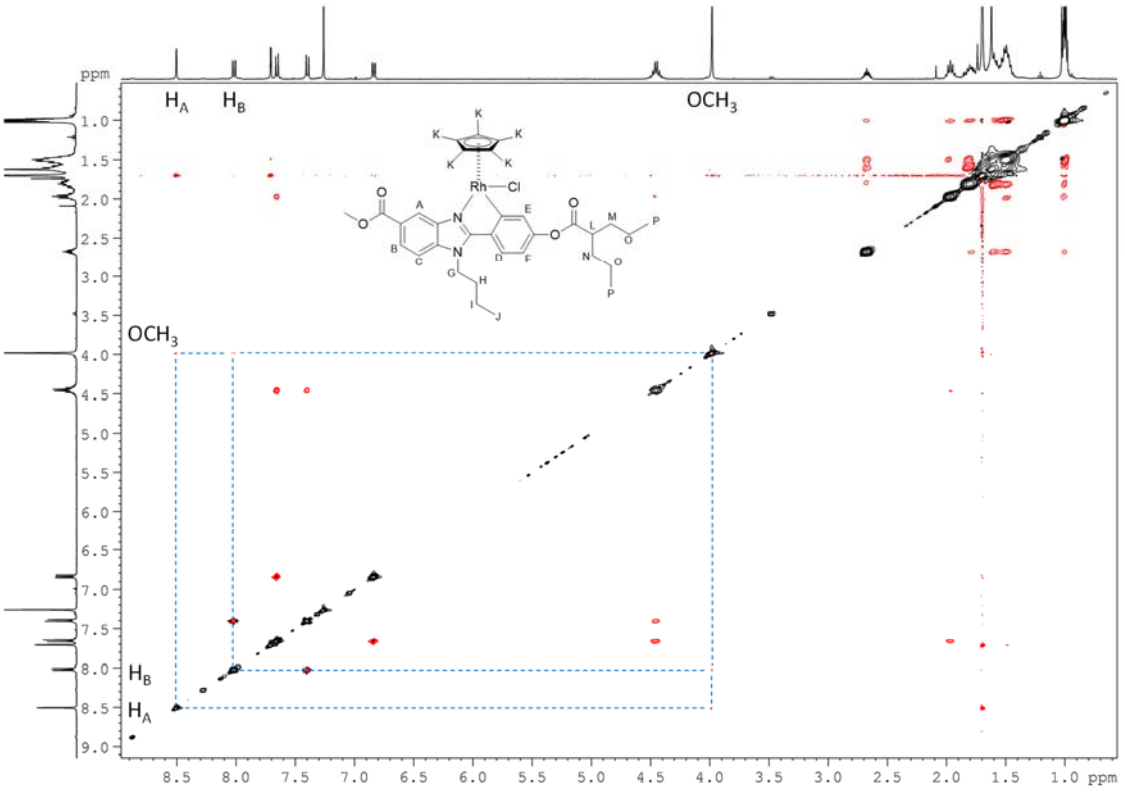

Figure S24. NOESY 2D ^{1}H-^{1}H NMR spectrum of **RhL2**, 400 MHz, $CDCl_3$.

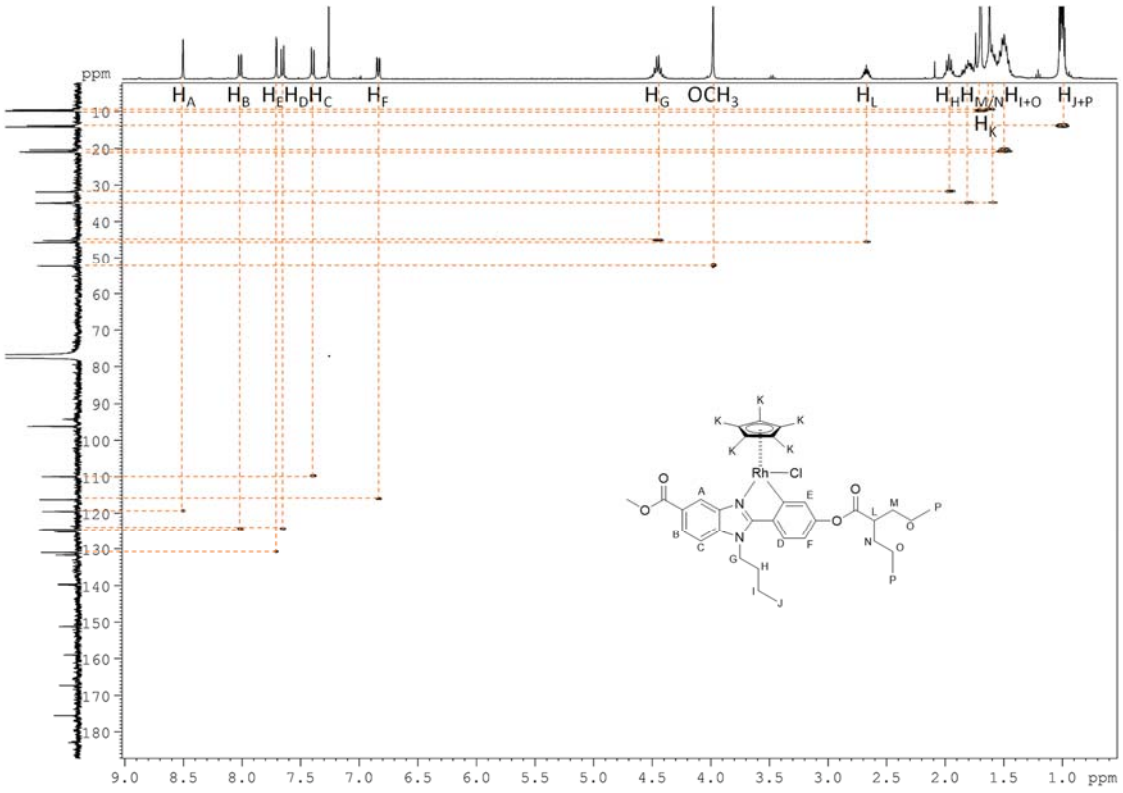

Figure S25. HSQC 2D ^{1}H-^{13}C NMR spectrum of **RhL2**, 400 MHz, $CDCl_3$.

4. Mass spectrometry

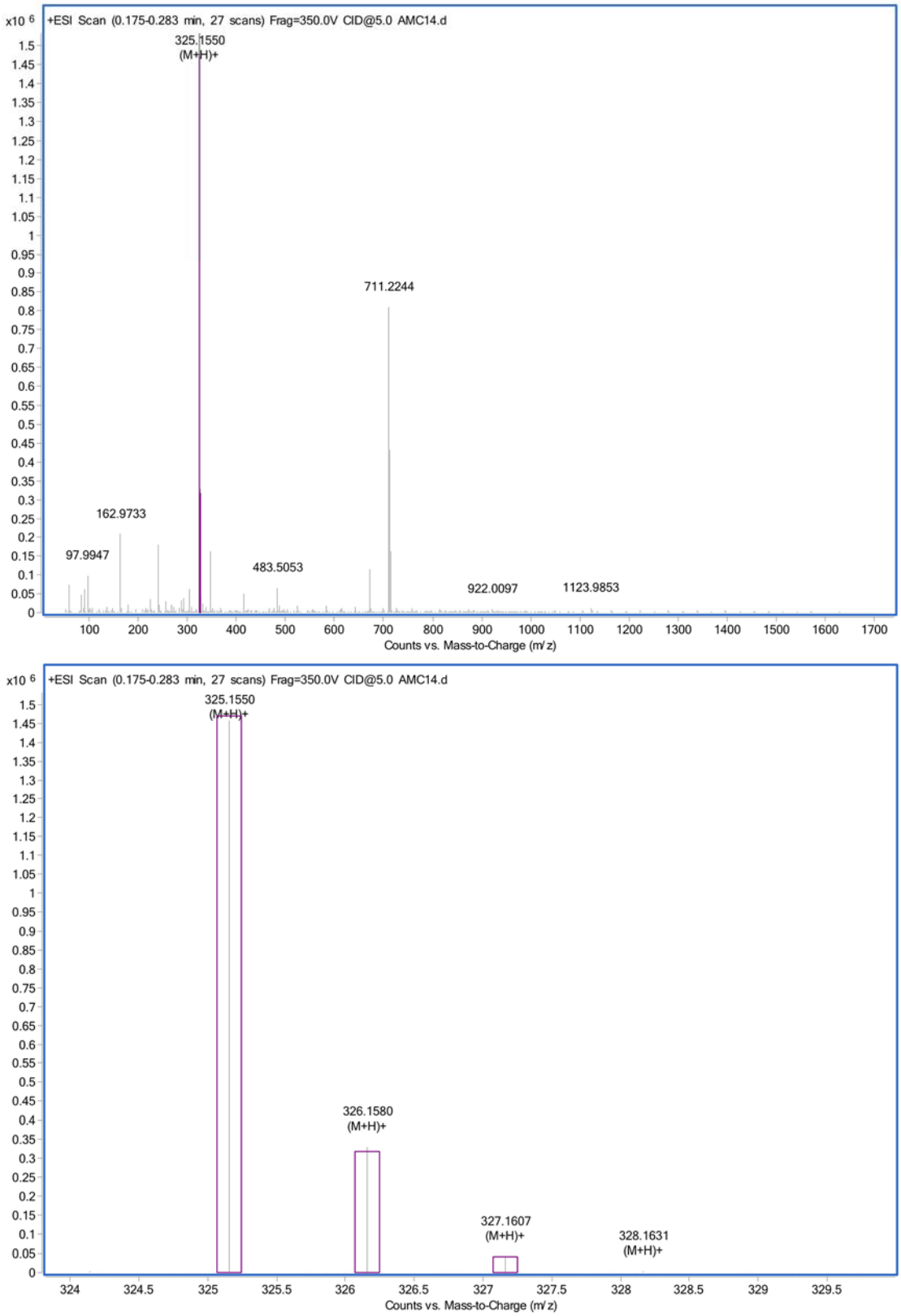

Figure S26. ESI-MS spectrum of **HL1** (positive detection mode).

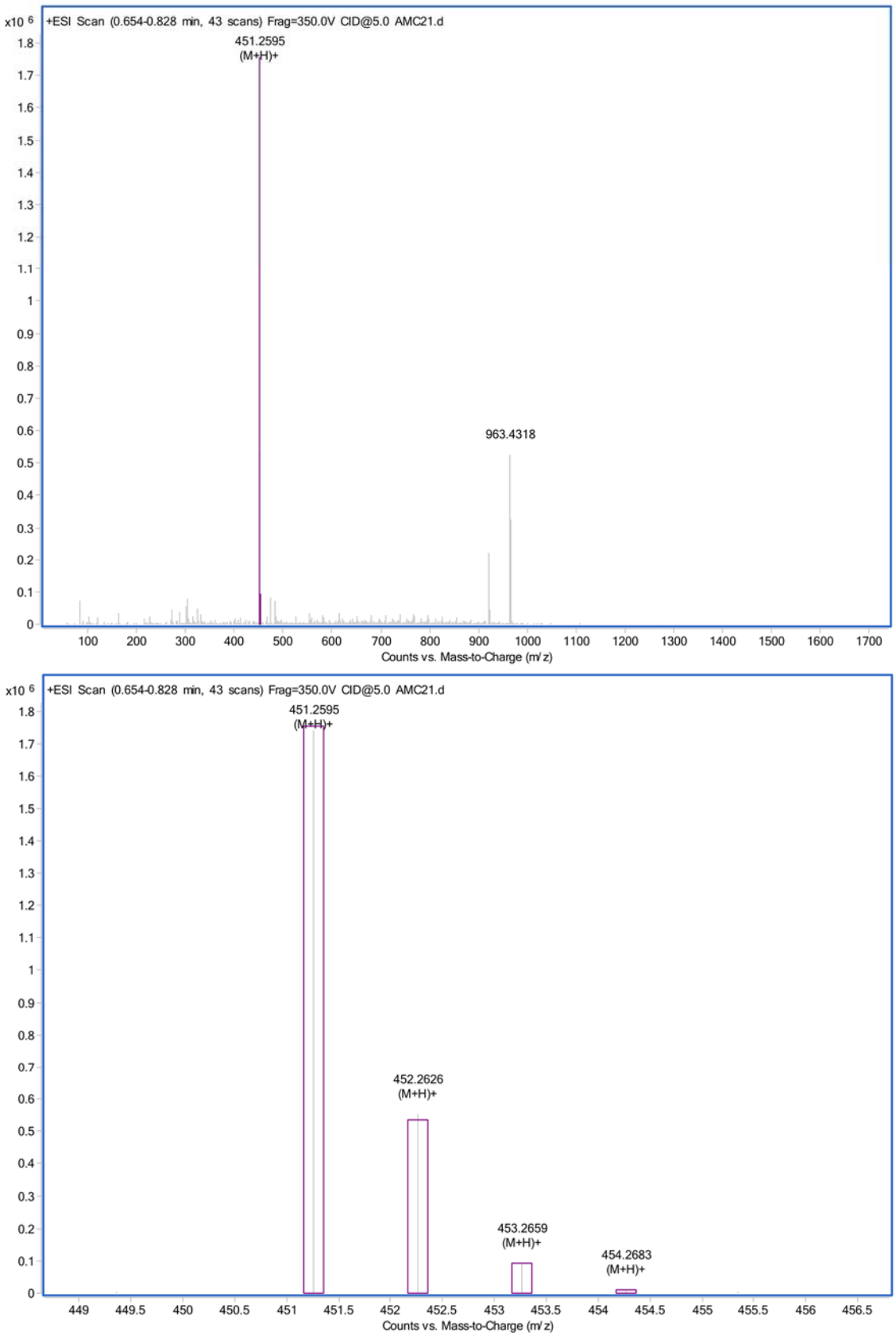

Figure S27. ESI-MS spectrum of **HL2** (positive detection mode).

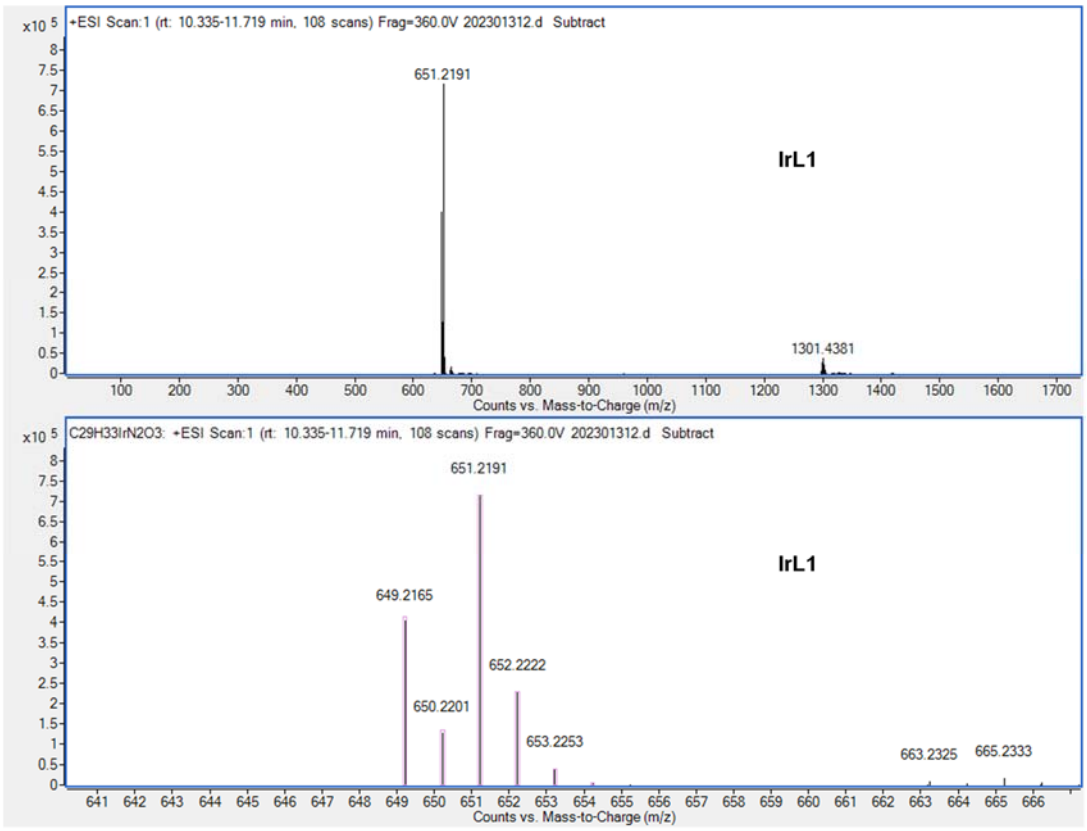

Figure S28. ESI-MS spectrum of **IrL1** (positive detection mode).

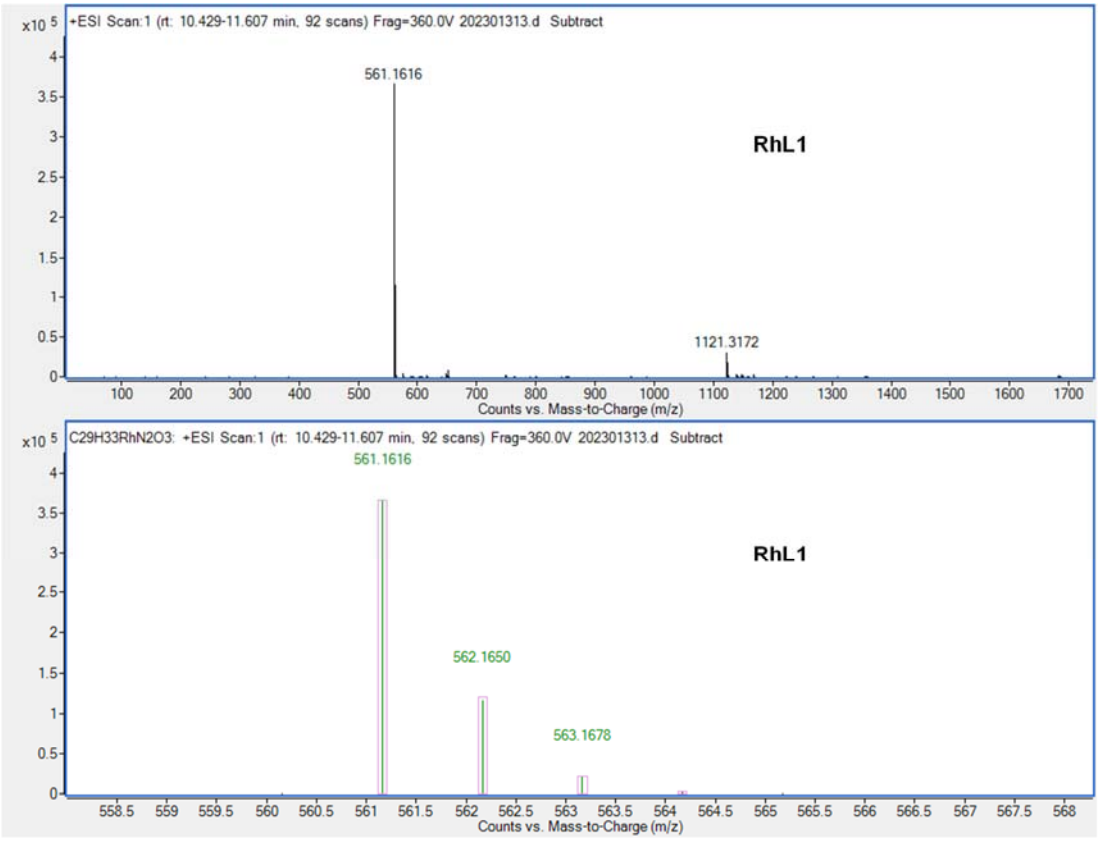

Figure S29. ESI-MS spectrum of **RhL1** (positive detection mode).

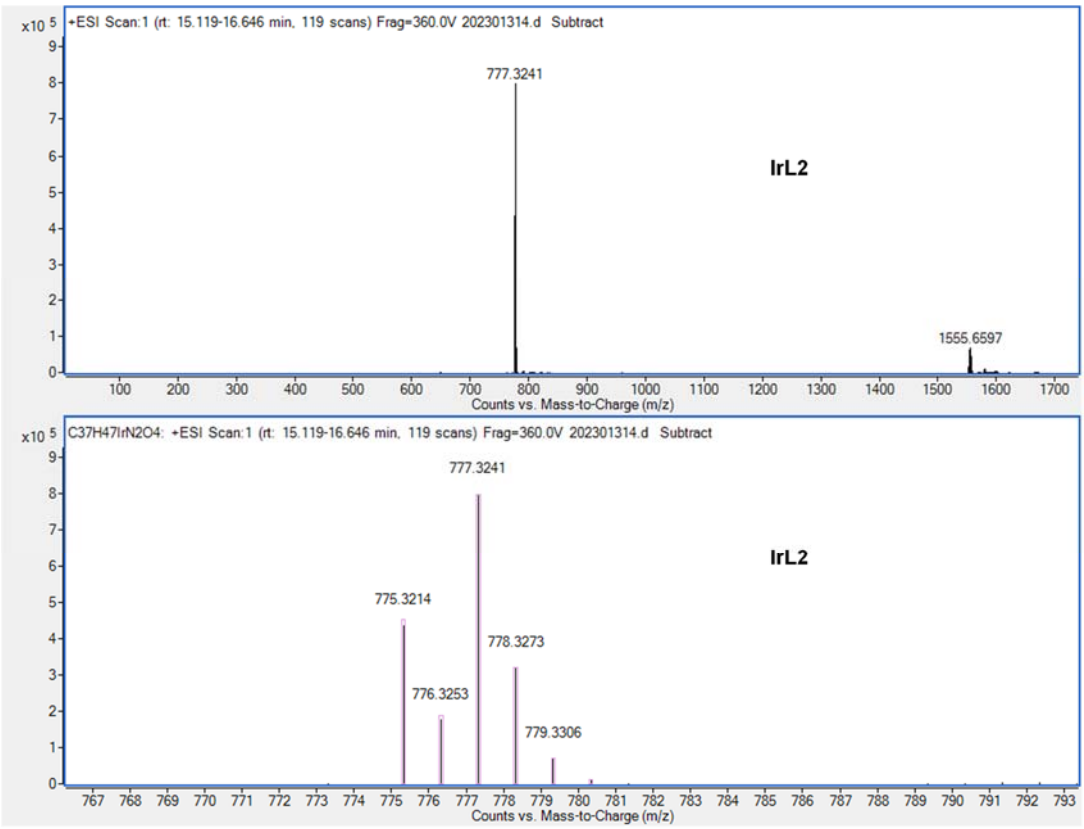

Figure S30. ESI-MS spectrum of **IrL2** (positive detection mode).

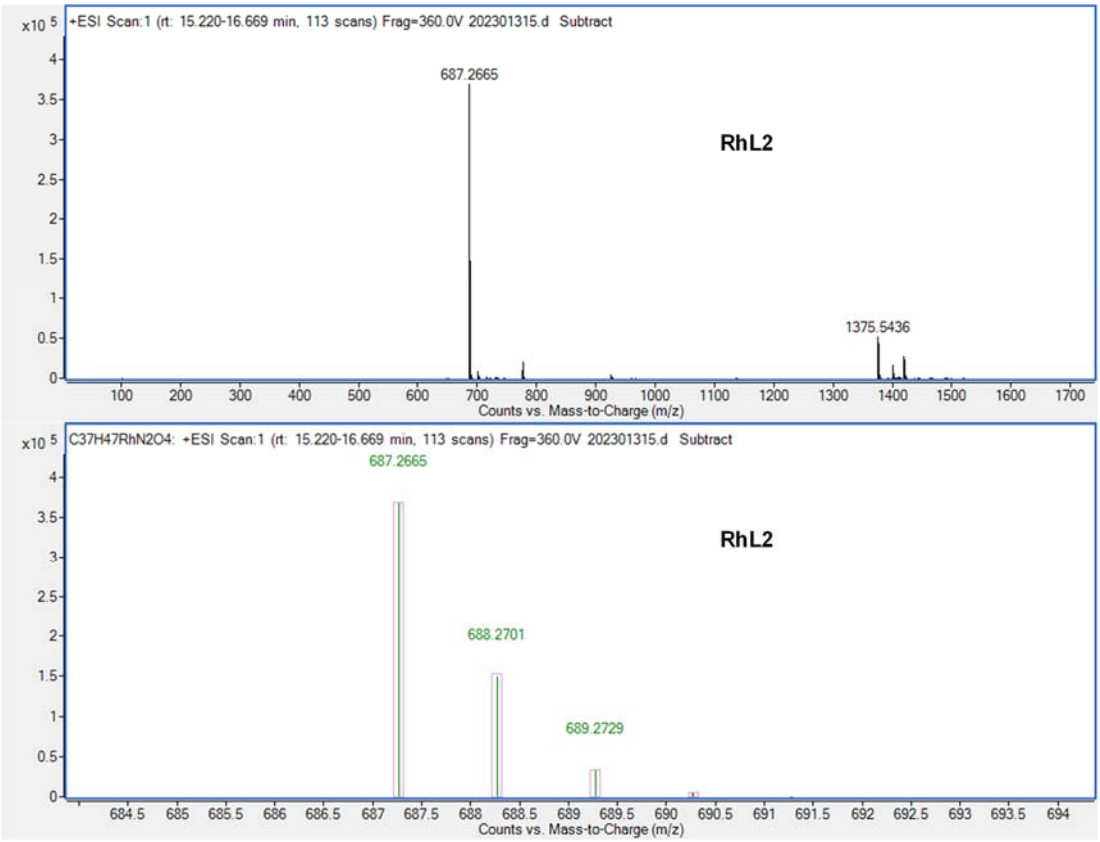

Figure S31. ESI-MS spectrum of **RhL2** (positive detection mode).

5. RP-HPLC of the complexes

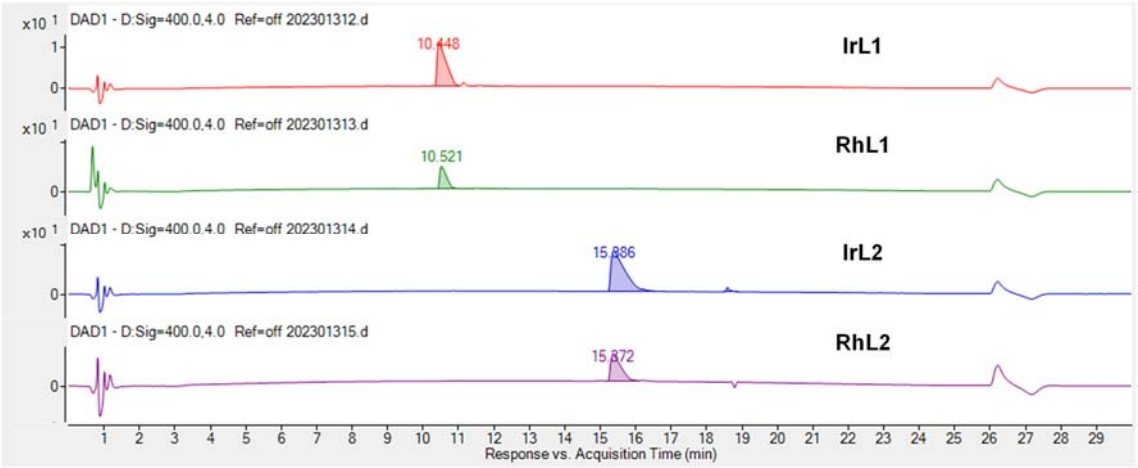

Figure S32. HPLC of complexes in DMF.

6. UV/Vis spectra

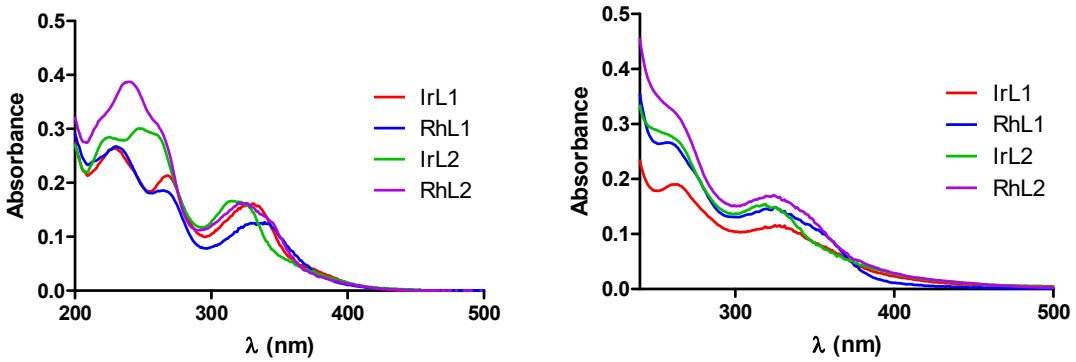

Figure S33. Visible spectra of complexes in acetonitrile and water (1% DMF), 10 μM.

7. Stability study

Stability in DMSO-d_6 by NMR

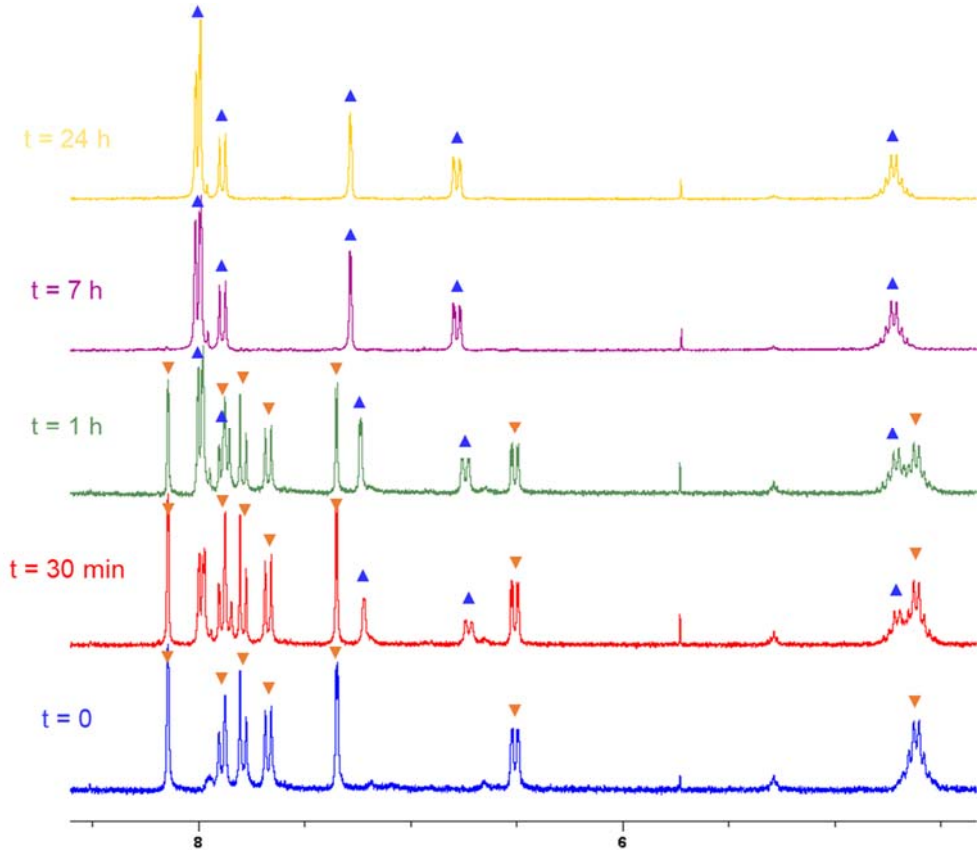

Figure S34. Stability of complex **IrL1** in DMSO-d_6 by ^{1}H NMR at t= 0, 30 min and 1, 7 and 24 hours at r. t.

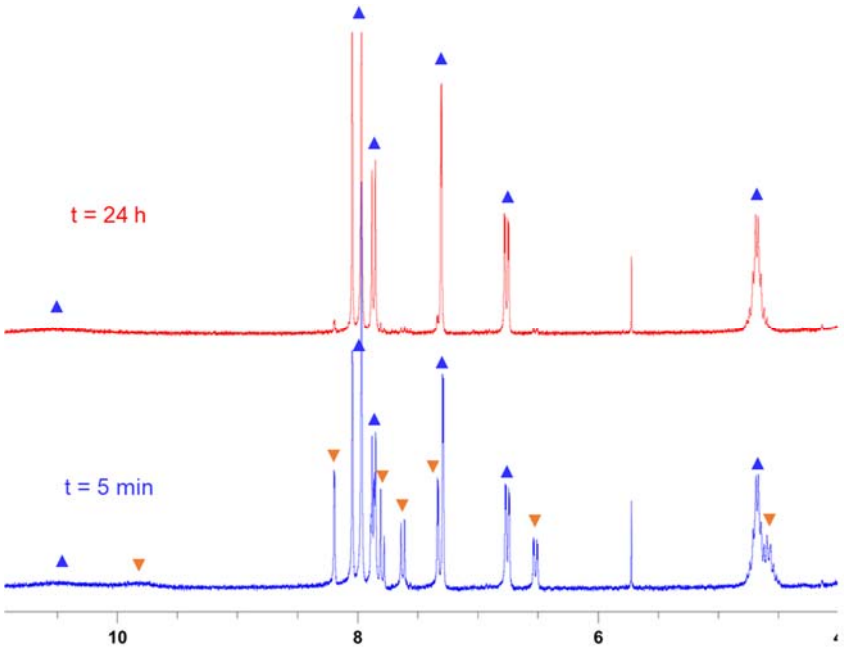

Figure S35. Stability of complex **RhL1** in DMSO-d_6 by ^{1}H NMR at t= 5 min and after 24 hours at r. t.

Stability in DMF-d_7 by NMR

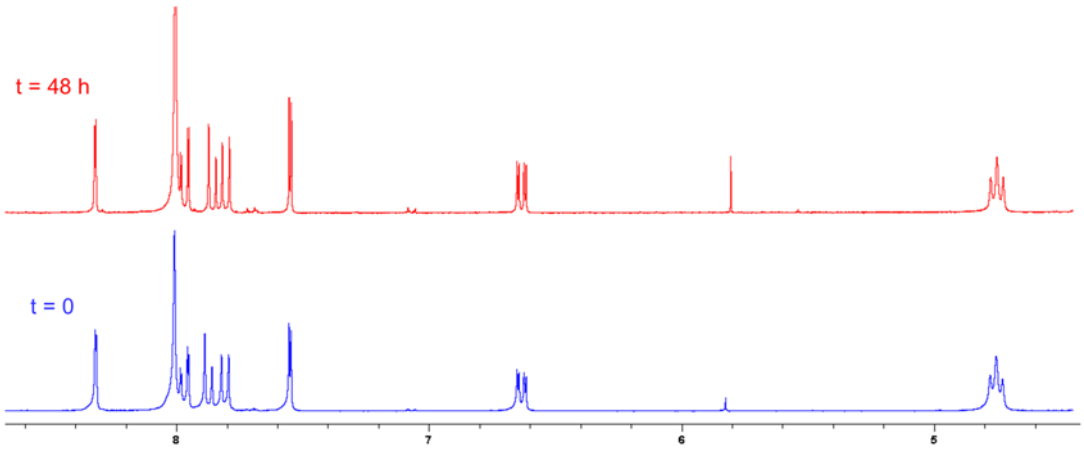

Figure S36. Stability of complex **IrL1** in DMF-d_7 by ^{1}H NMR after 48 hours at r. t.

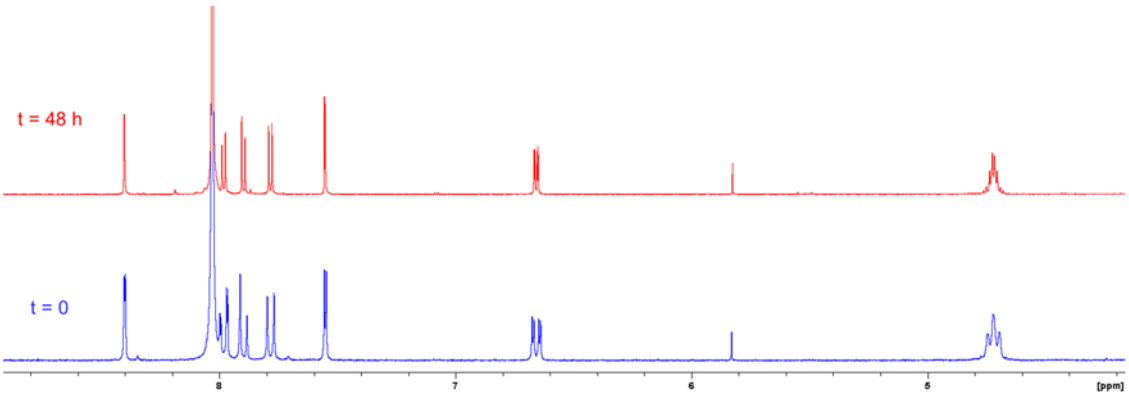

Figure S37. Stability of complex **RhL1** in DMF-d_7 by ^{1}H NMR after 48 hours at r. t.

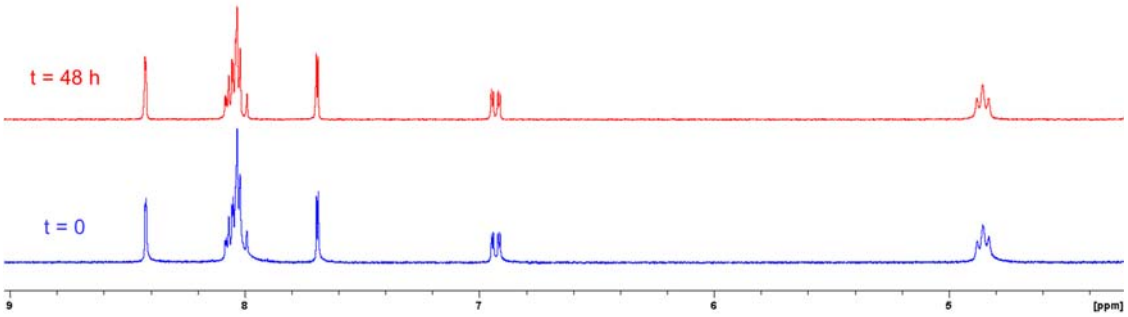

Figure S38. Stability of complex **IrL2** in DMF-d_7 by ^{1}H NMR after 48 hours at r. t.

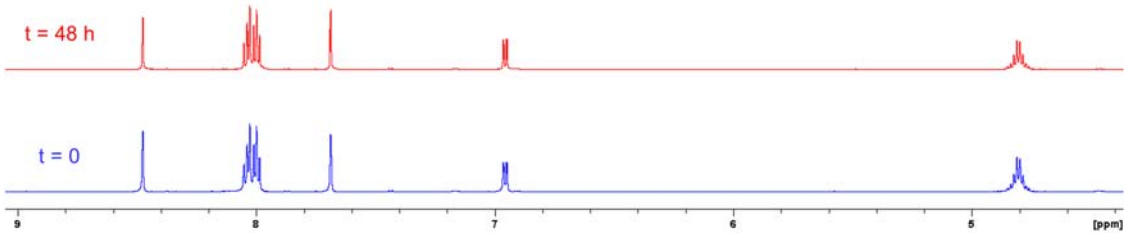

Figure S39. Stability of complex **RhL2** in DMF-d_7 by ^{1}H NMR after 48 hours at r. t.

Stability in RPMI (5% DMF) by UV/Vis

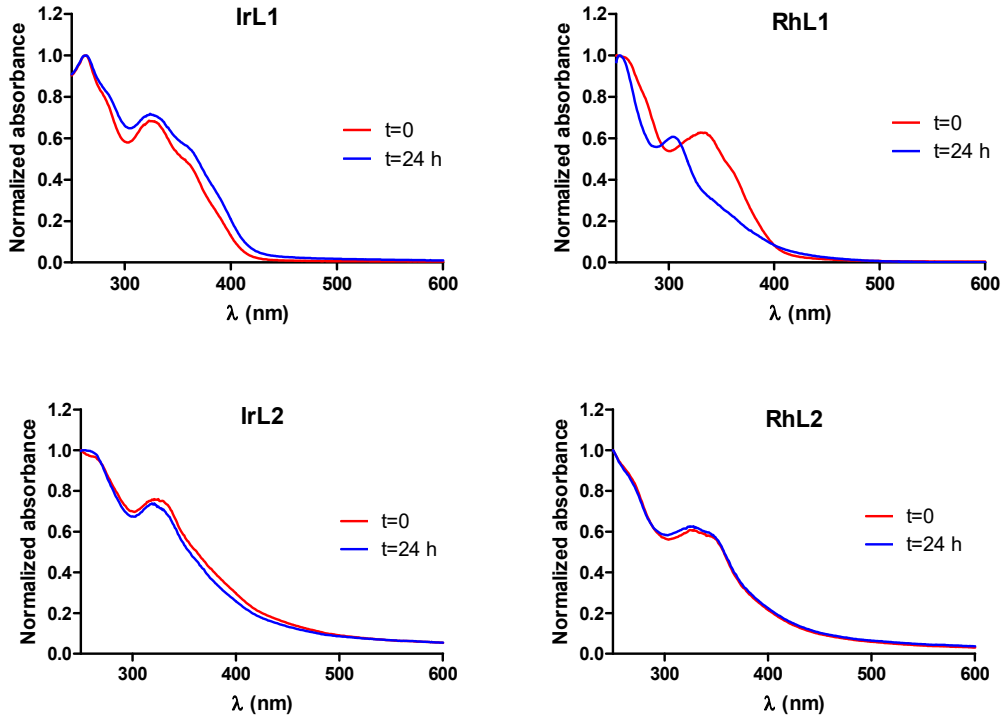

Figure S40. Stability of complexes in RPMI (5% DMSO) (10 μM) by UV/Vis after 24 hours of incubation at 37 ºC.

8. Hydrolysis study of complex RhL2 by NMR

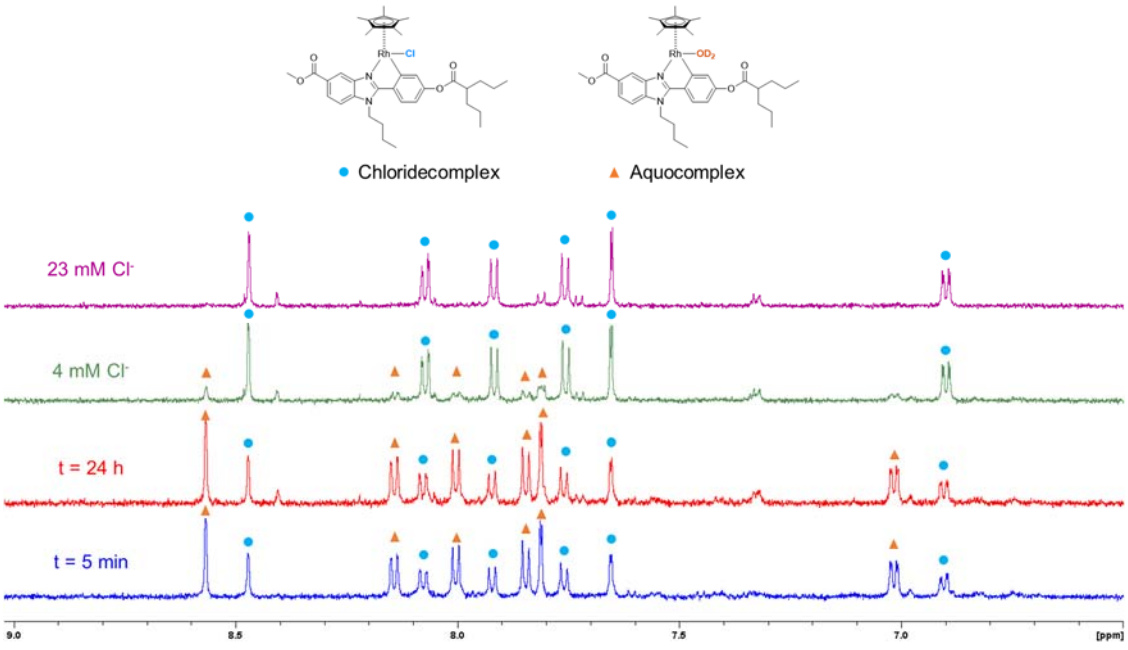

Figure S41. Hydrolysis study of complex **RhL2** 1 mM in MeOD:D_2O (2:1) by ^1H NMR, 600 MHz at r.t. After 5 min (blue line), after 24 hours (red line), after 24 hours and the addition of Cl^- (4 mM) (green line) and after 24 hours and the addition of Cl^- (23 mM) (purple line).

9. X-Ray crystallographic analysis for RhL2

X-Ray Structure Determinations. Intensities were registered at low temperature on a Bruker D8QUEST diffractometer using monochromated Mo *K*α radiation (λ = 0.71073Å). Absorption corrections were based on multi-scans (program SADABS).[5] Structures were refined anisotropically using SHELXL-2018.[6] Hydrogen atoms were included using rigid methyl groups or a riding model.

Table S2. Crystal data and structure refinement for AMC_23_0msp_a.

Identification code	AMC_23_0msp_a	
Empirical formula	C37 H48 Cl N2 O4 Rh	
Formula weight	723.13	
Temperature	100(2) K	
Wavelength	0.71073 Å	
Crystal system	Triclinic	
Space group	P-1	
Unit cell dimensions	a = 10.8394(5) Å	α= 105.159(2)°.
	b = 11.3065(6) Å	β= 94.760(2)°.

	c = 14.4856(7) Å γ = 90.872(2)°.
Volume	1706.35(15) $Å^3$
Z	2
Density (calculated)	1.407 Mg/m^3
Absorption coefficient	0.620 mm^{-1}
F(000)	756
Crystal size	0.240 x 0.220 x 0.090 mm^3
Theta range for data collection	1.867 to 30.619°.
Index ranges	-15<=h<=15, -16<=k<=16, -20<=l<=20
Reflections collected	154428
Independent reflections	10495 [R(int) = 0.0316]
Completeness to theta = 25.242°	100.0 %
Absorption correction	Semi-empirical from equivalents
Max. and min. transmission	0.746 and 0.6997
Refinement method	Full-matrix least-squares on F^2
Data / restraints / parameters	10495 / 0 / 415
Goodness-of-fit on F^2	1.219
Final R indices [I>2sigma(I)]	R1 = 0.0260, wR2 = 0.0561
R indices (all data)	R1 = 0.0311, wR2 = 0.0612
Largest diff. peak and hole	1.298 and -0.638 $e.Å^{-3}$

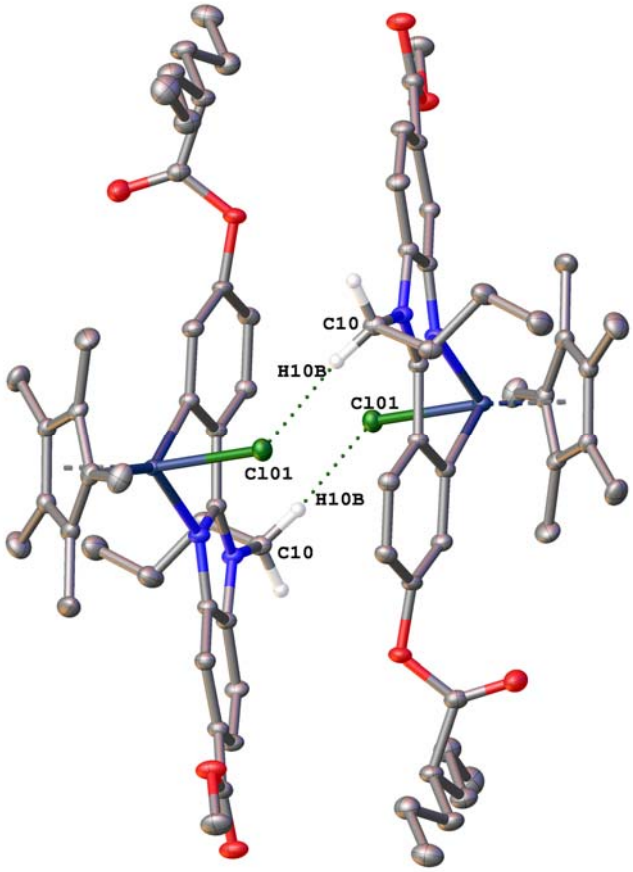

Figure S42. Hydrogen bonds for the complex **RhL2**.

10. Antibacterial activity: MIC and MBC determination.

Bacterial strains: *S. aureus* CECT 5190 (methicillin resistant, Gram positive bacteria), *A. baumannii* ATCC 17978 (Gram negative bacteria) and *P. aeruginosa* PAO1 (Gram negative bacteria) were maintained in Mueller–Hinton (MH) broth or agar at 37 °C whereas *E. faecium* CECT 5253 (vancomycin resistant, Gram positive bacteria) was maintained in tryptic soy (TS) broth or agar.

Minimum Inhibitory concentration (MIC) determination was performed according to the broth microdilution plate method following CLSI criteria (Performance standards for antimicrobial susceptibility testing: 17th informational supplement M07-A9, Clinical and Laboratory Standards Institute., 2012) as previously described.[7] The reported MIC values are the mean values of at least two independent experiments with four replicates.

Minimum bactericidal concentrations (MBC) were determined by plating 10 µL of the sample solutions from each well with no visible growth in MIC determination plates in MHA and then, by counting the number of colonies after 20 h of incubation at 37 °C. The concentration at which no colonies were grown corresponds to the MBC values.

11. Accumulation of metal complexes in bacteria

Bacterial inocula in the log phase were adjusted to 0.5 McFarland and then diluted 1: 100 in conical tubes with 5 mL of fresh MHB and 1 μM of the metal complexes. After overnight incubation at 37 °C and 120 rpm, samples were centrifuged at 8000 rpm for 10 min. The pellet was washed twice with phosphate buffered saline (PBS) and finally, resuspended in 1 mL of PBS. 20 μL were used to record the OD_{600} with a microplate reader (Cytation 5 cell imaging multi-mode reader (Biotek Instruments, USA)). Then, samples were diluted in 3 mL of MilliQ water and digested with 65% HNO_3 for 24 h before the analysis with an 8900 ICP-MS (Agilent Technologies). Data are reported as the mean of two independent experiments with two replicates for each condition assayed.

12. References

(1) Yellol, J.; Pérez, S. A.; Buceta, A.; Yellol, G.; Donaire, A.; Szumlas, P.; Bednarski, P. J.; Makhloufi, G.; Janiak, C.; Espinosa, A.; Ruiz, J. Novel C,N-Cyclometalated Benzimidazole Ruthenium(II) and Iridium(III) Complexes as Antitumor and Antiangiogenic Agents: A Structure–Activity Relationship Study. *J. Med. Chem.* **2015**, *58* (18), 7310–7327. https://doi.org/10.1021/acs.jmedchem.5b01194.

(2) Betti, M.; Genesio, E.; Marconi, G.; Sanna Coccone, S.; Wiedenau, P. A Scalable Route to the SMO Receptor Antagonist SEN826: Benzimidazole Synthesis via Enhanced in Situ Formation of the Bisulfite–Aldehyde Complex. *Org. Process Res. Dev.* **2014**, *18* (6), 699–708. https://doi.org/10.1021/op4002092.

(3) Ye, R.-R.; Cao, J.-J.; Tan, C.-P.; Ji, L.-N.; Mao, Z.-W. Valproic Acid-Functionalized Cyclometalated Iridium(III) Complexes as Mitochondria-Targeting Anticancer Agents. *Chemistry – A European Journal* **2017**, *23* (60), 15166–15176. https://doi.org/10.1002/chem.201703157.

(4) Yellol, G. S.; Donaire, A.; Yellol, J. G.; Vasylyeva, V.; Janiak, C.; Ruiz, J. On the Antitumor Properties of Novel Cyclometalated Benzimidazole Ru(Ii), Ir(Iii) and Rh(Iii) Complexes. *Chem. Commun.* **2013**, *49* (98), 11533. https://doi.org/10.1039/c3cc46239k.

(5) Bruker. Bruker; AXS Inc.: Madison, Wisconsin, USA, 2001.

(6) Sheldrick, G. M. Crystal Structure Refinement with *SHELXL*. *Acta Crystallogr C Struct Chem* **2015**, *71* (1), 3–8. https://doi.org/10.1107/S2053229614024218.

(7) Busto, N.; Vigueras, G.; Cutillas, N.; García, B.; Ruiz, J. Inert Cationic Iridium(III) Complexes with Phenanthroline-Based Ligands: Application in Antimicrobial Inactivation of Multidrug-Resistant Bacterial Strains. *Dalton Trans.* **2022**, *51* (25), 9653–9663. https://doi.org/10.1039/D2DT00752E.